Mitochondrial metabolism in the spotlight. Keeping of the balanced RNAP III activity ensures cellular homeostasis.

Roza Szatkowska , Emil Furmanek , Andrzej Kierzek , Christian Ludwig , Malgorzata Adamczyk *

Posted Date: 26 July 2023

doi: 10.20944/preprints202307.1751.v1

Keywords: RNA Polymerase III, RNAP III, TCA cycle, mitochondrial metabolism, MAF1, 13C flux, systems biology, growth rate

Article

Mitochondrial Metabolism in the Spotlight. Keeping of the Balanced RNAP III Activity Ensures Cellular Homeostasis

Roza Szatkowska [1], Emil Furmanek [1], Andrzej Kierzek [2,3], Christian Ludwig [4] and Malgorzata Adamczyk [1,*]

[1] Laboratory of Systems and Synthetic Biology, Chair of Drugs and Cosmetic Biotechnology, Warsaw University of Technology, Poland
[2] Certara UK, Sheffield, United Kingdom
[3] School of Biosciences and Medicine, University of Surrey, Guildford, United Kingdom
[4] Institute of Metabolism and Systems Research, University of Birmingham, UK
* Correspondence: malgorzata_adamczyk@pw.edu.pl

Abstract: RNA polymerase III (RNAP III) holoenzyme activity and its products processing have been linked to several metabolic dysfunction in lower and in higher eukaryotes. Alterations in the activity of RNAP III driven synthesis of non-coding RNA, causes extensive changes in the glucose metabolism. Increased RNAP III activity in *S.cerevisiae maf1Δ* strain, manifests with lethality when grown on non-fermentable carbon source. This lethal phenotype is suppressed by reducing tRNA synthesis. The cause for the lack of growth neither the underlying molecular mechanism has not been deciphered and has been awaiting a scientific explanation for a decade. Our previous proteomics data suggested mitochondrial dysfunction of the strain. Using model mutant strains *maf1Δ* (with increased tRNA abundance) and *rpc128-1007* (with reduced tRNA abundance) we collected data showing major changes in TCA cycle metabolism of the mutants that explain the phenotypic observations. The present study, based on ^{13}C flux data and analysis of TCA enzymes activities, identifies the flux constraints in the mitochondrial metabolic network. The lack of growth is associated with the decrease in TCA cycle activity and downregulation of the flux towards glutamate, aspartate and phosphoenolopyruvate (PEP), the metabolic intermediate feeding gluconeogenic pathway. *rpc128-1007*, the strain that is unable to increase tRNA synthesis due to a mutation in C128 subunit, has increased activity of TCA cycle under non-fermentable conditions. To summarize, cells with non-optimal activity of RNAP III, undergo substantial adaptation to a new metabolic state, that make them vulnerable under specific growth conditions. Our results strongly suggest that balanced, non-coding RNA synthesis that is coupled to glucose signaling is a fundamental requirement to sustain cell's intracellular homeostasis and flexibility under changing growth conditions. Presented results provide insight into the possible role of RNAP III in mitochondrial metabolism of other cell types.

Keywords: RNA Polymerase III; RNAP III; TCA cycle; mitochondrial metabolism; MAF1; ^{13}C flux; systems biology; growth rate

1. Introduction

Mitochondria are considered the major source of energy production and signaling hub [1]. When mitochondrial biological function is compromised, this follows with dysfunction in cellular homeostasis leading to aging and disease. Over the recent years the mechanism of action of RNA polymerase III (RNAP III) has been researched extensively but rarely in relation to metabolic homeostasis, neither specifically to mitochondrial metabolism [2]. Primarily RNAP III is responsible for the synthesis of non-coding RNAs, including tRNA, U6 snRNA, 5S rRNA, 7SL RNA and the RNA component of ribonuclease P (RNase P) [3,4]. The activity of this enzyme is inhibited by evolutionary

 doi:10.20944/preprints202307.1751.v1

conserved regulator, the Maf1 protein, in response to intra- and extracellular signals such as carbon source change, entry into stationary growth phase, DNA damage, oxidative stress, or cell treatment with rapamycin or chlorpromazine [5–11]. The Maf1 protein is the only negative regulator of RNAP III in the *Saccharomyces cerevisiae* [5]. Consequently, Maf1 deficient cells (*maf1Δ*) show higher RNAP III activity, leading to the increased levels of some classes of tRNAs and their precursors decoupled from environmental clues [2]. Apart from the function in the process of tRNA transcription, high RNAP III activity is negatively corelated with the activity of high affinity glucose transporters and positively corelated with glycolytic pathway activity in *S.cerevisiae* [12,13]. Furthermore, the increased activity of RNAP III by the deletion of MAF1 gene causes a growth defect on non-fermentable carbon source at 37°C, which has been linked to gluconeogenesis [14]. However, the hypothesis of downregulation of FBP1 transcriptional activity, that may lead to decreased fructose bisphosphatase levels, as the causative factor of the putative impairment of gluconeogenis activity in *maf1Δ* has been already challenged [13,15,16]. *maf1Δ* phenotype is reversed by a point mutation [resulting in a replacement of a glycine with alanine at position 1007 in C128 which is the second largest subunit of RNAP III [17]. The point mutation carried by *rpc128 1007* leads the limited ability of this mutant to use glucose as a carbon source and significant induction of GCN4 regulated genes [12,13]. Maf1 deficient cells show a metabolic profile similar to some cancer cells that display the Warburg effect. Upregulated RNAP III activity causes cells to reprogram their metabolism towards increased activity of glycolytic enzymes when grown under high glucose conditions as shown by Szatkowska et al. [13]. The glucose flux is also redirected towards the pentose phosphate pathway, glycogen and trehalose shunt in *maf1Δ* [13]. On contrary, in the *rpc128-1007* strain [with low RNAP III activity] the activities of all glycolytic enzymes are reduced [13]. This is correlated with a drastic inhibition of glucose metabolism and a change in the transcription profile of glucose transporters [12].

Similarly, to *maf1Δ* phenotype, null mutants of ADH1, SDH1, SDH2, SDH3, SDH4, FUM1 genes do not grow on glycerol as a carbon source [18]. Therefore, being guided by our proteomics data, we aimed at deciphering, whether the tricarboxylic acid cycle (TCA) activity is impaired in Maf1 deficient cells on glucose, glycerol and after temperature shift or not. This implication was additionally supported by the fact, that the point mutation in C128 subunit of RNAP III restores the ability of *maf1Δ* to effectively utilize glycerol at 37°C in the double mutant *maf1Δ rpc128-1007*.

The main goal of the presented study was to assess the relative importance of the TCA cycle in S. cerevisiae strains that differ in the activity of RNAP III under fermentative and respiratory growth conditions to explain the lack of *maf1Δ* growth on respiratory carbon source at non-permissive temperature. Additionally, we aimed at understanding the survival strategy of its suppressor, *rpc128-1007*, under conditions, when the only available source of carbon is the glucose.

In this work we show that the metabolism of the *rpc128-1007* strain, decoupled from glucose signaling in the presence of carbon source [12], relies on Idp dependent reductive carboxylation of glutamine as the primary energy source, even though glucose is abundant. The low growth rate does not increase TCA cycle activity. Both mutants (*maf1Δ* and *rpc128-1007*) show a decrease in TCA cycle activity during fermentative growth. In note, both mutants accumulate acetylo-CoA. The observed changes in TCA cycle activity measured by ^{13}C flux approach that are further supported with enzymatic assays are further reflected in the changes of NAD+/NADH ratios under both growth conditions studied here.

2. Results

2.1. ^{13}C flux through TCA cycle is affected indirectly by RNAP III activity on glucose

To test the intracellular distribution of carbon flow through the TCA cycle in *maf1Δ* and *rpc128-1007* yeast strains, the NMR detected ^{13}C isotopomer distribution in amino acids from ^{13}C-labelling experiments was analyzed. For this purpose, different isotopic tracers, [U-^{13}C] glycerol and [1,2-^{13}C] glucose, were used.

The citric acid cycle is a source of the carbon backbone for ten amino acids [19]. Thus, labelling distribution in amino acid pools depends on the ^{13}C profile of TCA cycle intermediates. Alanine is

Preprints (www.preprints.org) | NOT PEER-REVIEWED | Posted: 26 July 2023 doi:10.20944/preprints202307.1751.v1

used as a reporter molecule on isotopic labelling in pyruvate – the end metabolite of the glycolytic pathway. This approach was taken, due to difficulties in measuring pyruvate levels by 2D-^{1}H,^{13}C HSQC NMR spectroscopy. When labelled alanine was observed, this enabled the estimation of the carbon flux before pyruvate enters the TCA cycle. Splitting of carbon labelling into alanine isotopomers gives the information on the positioning of the isotopic atoms in the end-product of glycolysis, which is pyruvate. In the case of *rpc128-1007* higher concentration of [3-^{13}C] alanine could be observed, which means, that this isotopomer might originate from PPP pathway.

While [1,2-^{13}C] acetyl-CoA results in [4,5-^{13}C] glutamate when generated directly from α-ketoglutarate via transamination, a full round of TCA cycle activity moves this label into [3-^{13}C] and [1,2-^{13}C]-labelled glutamate isotopomers. While glutamate is not a TCA cycle intermediate, it is a very good reporter of TCA cycle activity due to its high abundance. Specific isotopomers allow to conclude on relative pathway activities and flux distribution.

Except to outflow of intermediates to support the biosynthesis of glutamate, the carbon flux into aspartate synthesis in rpc128-1007 on glucose as well in maf1Δ as indicated by relative percentage fold change of [3,4-^{13}C] and [2,3-^{13}C] aspartate (Figure 1D,E) is not greatly perturbed. No change in PHD derived [3,4-^{13}C] aspartate seems explicit. While the presence of [2,3-^{13}C] aspartate, observed in rpc128-1007, suggests that aspartate is mostly synthesized here via an anaplerotic pathway (Figure 1E), via oxaloacetate branch, formed directly from pyruvate by the pyruvate carboxylase (Pyc1). In the strain with compromised RNAP III activity, the carbon flow through Pyc1, supports the formation of asparatate and in the contrast to maf1Δ (Figure 1D). In rpc128-1007 Pyc1 mediated pathway is dominant while directing this carbon backbone towards sustained glutamate synthesis [2,3-^{13}C] glutamate and [2,3,4,5-^{13}C] glutamate (Figure 1G).

To conclude, both, the increase as well the decrease in RNAP III capacity correlate with a changes in TCA efficiency under fermentative conditions, that is a decrease in flux, that supports our previously published data [13]. The flux into aspartate is sustained. Different dependencies can be observed under respiratory growth supported with glycerol as the carbon source, which is supported by data presented in the following sections.

Preprints (www.preprints.org) | NOT PEER-REVIEWED | Posted: 26 July 2023 doi:10.20944/preprints202307.1751.v1

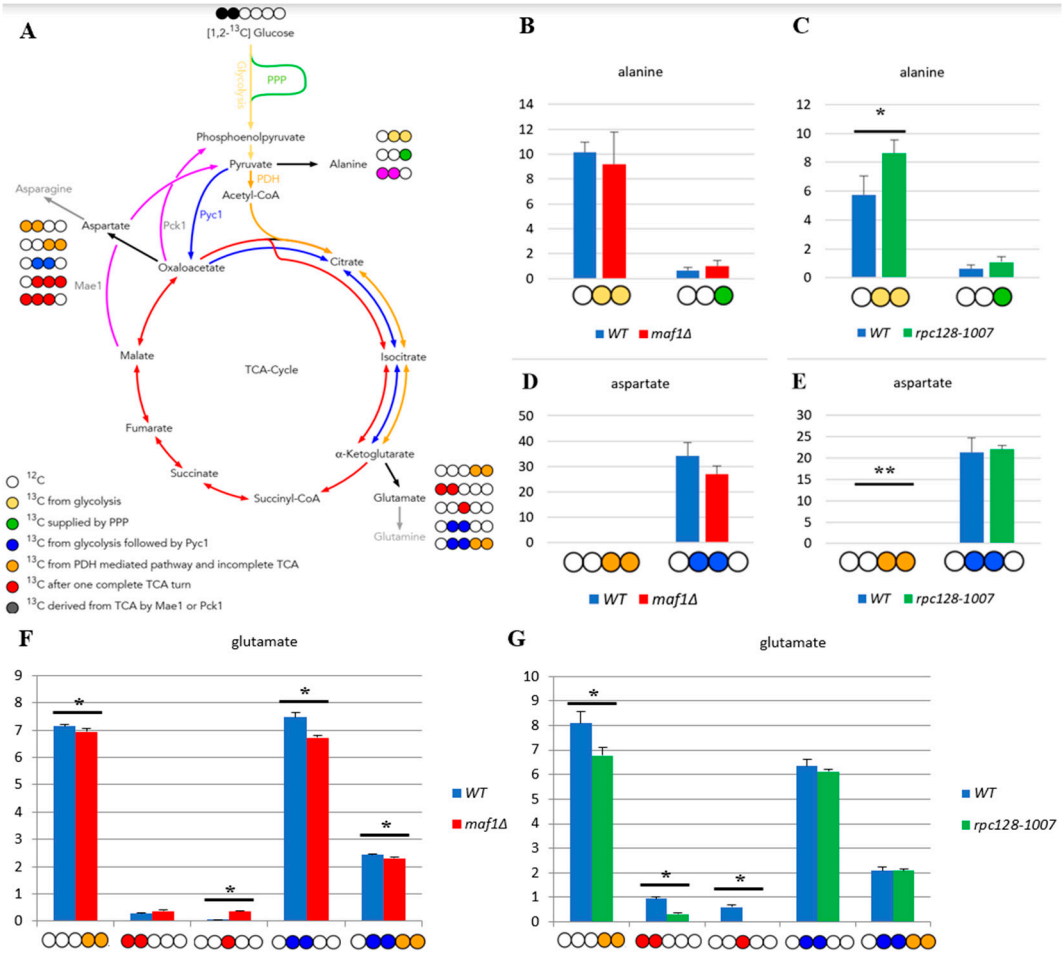

Figure 1. MAF1 deletion and C128 point mutant have less active TCA cycle than WT during fermentative growth. (A) Schematic simplified diagram of the possible incorporation of ^{13}C atoms from [1,2-^{13}C] glucose to isotopomers of alanine and glutamate. Carbon atoms are shown as circles. Filled circles represent ^{13}C and empty circles - 12C atoms. Yellow circle stands for ^{13}C derived from glycolysis. Green circle marks atom supplied by pentose phosphate pathway (PPP). Blue circle represents labelling derived from glycolytic pyruvate followed by anaplerotic reaction mediated by pyruvate carboxylase 1 (Pyc1) into TCA. Deep yellow circle shows ^{13}C obtained from acetyl-CoA formed from glycolytic pyruvate by pyruvate dehydrogenase complex (PDH) and exit the TCA before completion of one full cycle. Red circle symbolises the atom that left Krebs cycle after at least one complete turn. Pink stands for labelling that exited the TCA through cataplerotic pathways driven either by malic enzyme (Mae1) or by phosphoenolpyruvate carboxykinase (Pck1) into pyruvate. Colourful arrows symbolise the carbon flow that has led to specific labelling positions. White circle stands for the incorporation of 12C atoms. Alanine (B, C), aspartate (D, E) and glutamate (F, G) ^{13}C isotopomer percentage distributions in yeast strains with different RNAP III activity. Yeast cells were grown in rich medium (YP) supplemented with 2 % [1,2-^{13}C] glucose (YPD) until log phase. Cultures were grown overnight in YPD (B, D) or YPGly (C, E) medium. ^{13}C incorporation to amino acids isotopomers is marked as 1, while 0 stands for 12C atoms. Results are shown as mean alanine and glutamic acid isotopomer distribution with standard deviation (SD) for three independent biological replicates. The unlabelled amino acid pools (0 0 0 0 0) are not shown in the graph. Asterisk (*) indicates p-value < 0.05 according to Student's t-test.

The flux distribution data (Figure 1) suggest that both strains with altered RNAP III activity face a reduction of TCA cycle activity in comparison to the wild-type isogenic strain, when grown on glucose. The effect is rather mild in maf1Δ. This is clearly indicated by the labelling pattern of glutamine (Supplement Table S1), and especially by positional ^{13}C depletion in [4,5-^{13}C] and [2,3-^{13}C] glutamate isotopomers in glutamic acid labelled pool (Figure 1F,G) found in both mutants, showing

Preprints (www.preprints.org) | NOT PEER-REVIEWED | Posted: 26 July 2023 doi:10.20944/preprints202307.1751.v1

replenished flux towards completion of the cycle. However the increase in [3-^{13}C] glutamate indicates formation of glutamate after one complete TCA cycle in maf1Δ. This isotopomers is completely absent in NMR spectra in showing flux distribution in rpc128-1007. Depletion in [3-^{13}C], moreover [1,2-^{13}C] is observed in rpc128-1007. [3-^{13}C] and [1,2-^{13}C] glutamate isotopomers are synthesised, when the carbon backbone is converted before the α-ketoglutarate (AKG) leaves the citric acid cycle to be further converted into glutamate (Figure 1A) and consequently there are markers for sustained TCA cycle activity.

2.2. Lower flux toward glutamate in Maf1 deficient mutant can be compensated by its suppressor's high metabolic activity in glutamate synthesis.

The ^{13}C analysis clearly indicates that maf1Δ cells grown on glycerol at 30°C have down regulated activity of TCA (Figure 2). This effect is reversed by its phenotypic suppressor, rpc128-1007 via flux rewiring. The rpc128-1007 shows highly active TCA on non fermentable carbon source, which can be supported by an elevated biosynthesis of uniformly labelled glutamate (Figure 2D) that is formed after at least two full Krebs cycles. The data shows, that [1,2,3-^{13}C] glutamate [U-^{13}C] glutamate pool is lowered approximately by 5-fold in maf1Δ and [U-^{13}C] glutamate is not formed (Figure 2D). Moreover, in maf1Δ there is a significant decrease in [1,2-^{13}C] and [3- ^{13}C] glutamate pool, which are indicators of completion of at least one full TCA cycle. It's concentration shall still be above the detection level (Figure 2D)). Additionally, the downshift in [2,3,4- ^{13}C] aspartate isotopomer production indicates lower capacity of TCA cycle, which cannot be completed, in Maf1 deficient strain (Figure 2C). It is however worth noting, that asparate production is sustained in this mutant, synthesized along the route via PDH following the incomplete TCA cycle exemplified by [1, 2- ^{13}C] aspartate isotopomer, which indicates metabolites supply for nucleotides production (Figure 2C). The opposite activity of TCA is observed in maf1Δ suppressor strain (rpc128-1007). This indicates an inverse correlation between RNAP III activity and citric acid cycle efficiency under respiratory growth.

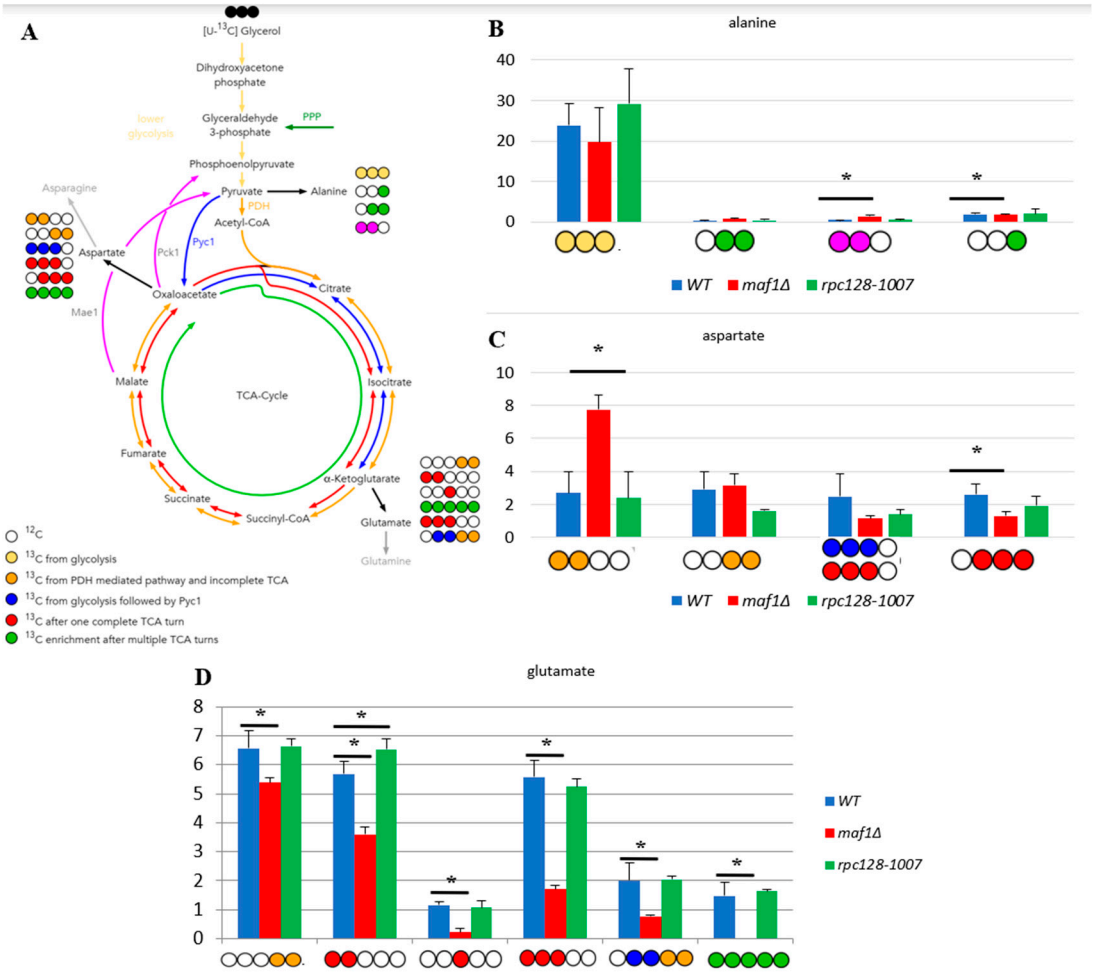

 doi:10.20944/preprints202307.1751.v1

Figure 2. Higher TCA activity in rpc128-1007 and lower in maf1Δ comparing to reference strain on glycerol-based medium**.** Alanine (B), aspartate (C), Glutamate (D) ^{13}C isotopomer percentage distributions in yeast strains with different RNAP III activity. Yeast cells were grown in rich medium (YP) supplemented with 2 % [U-^{13}C] glycerol (YPGly) (B, C, D) until log phase. Cultures were grown overnight in YPGly (B, C, D) medium. ^{13}C incorporation to glutamate and aspartate isotopomers is marked as 1, while 0 stands for 12C atoms. Results are shown as mean amino acids isotopomer distribution with standard deviation (SD) for three biological replicates. Asterisk (*) indicates p value < 0.05 according to Student's t-test. The unlabelled glutamic acid pool (0 0 0 0 0) is not shown in the graph. (A) Schematic simplified diagram of the possible incorporation of ^{13}C atoms from [U-^{13}C] glycerol to isotopomers of aspartate and glutamate. Carbon atoms are shown as circles. Filled circles represent ^{13}C and empty circles - 12C atoms. Blue circle represents labelling derived from glycolytic pyruvate followed by anaplerotic reaction mediated by Pyc1 into TCA. Deep yellow circle shows ^{13}C obtained from acetyl-CoA formed from glycolytic pyruvate by PDH and exit the TCA before completion of one full cycle. Red circle symbolises the atom that left Krebs cycle after at least one complete turn. Stripped red circle represents ^{13}C enrichment that achieved at least two full cycles of TCA before redirection of the carbon flow into biosynthesis pathways. Colourful arrows symbolise the carbon flow that has led to specific labelling positions. Asterisk (*) indicates p value ≤ 0.05 by Student's t test.

2.3. Elevated temperature along with non-fermentative glycerol further abolishes TCA cycle activity in maf1Δ

We intended to use ^{13}C flux analysis to precisely dissect metabolic alterations in maf1Δ that cause the growth defect on glycerol at 37°C. Therefore, cells carrying MAF1 deletion were grown on [U-^{13}C] glycerol as a carbon source at 30°C until OD600 ≈ 1.0 and measured the flux also after 1 h shift to 37°C, the conditions which causes the mutant lethality

We noticed, that the shift to elevated temperature in general slightly upregulates the citric acid cycle activity in both, wild-type and maf1Δ yeast strains when compared to the data obtained at 30°C (Figure 3B). The only exception was [1,2 -^{13}C] aspartate, which seemed to be enriched in maf1Δ grown at permissive temperature (Figure 2C compare to Figure 3C).

The most significant difference between maf1Δ metabolism at 30°C and 37°C, as we observed, was the consequent decrease in production of aspartate . maf1Δ grown on [U-^{13}C] glycerol after temperature shift produces less [1,2- ^{13}C] , [3,4- ^{13}C], [2,3- ^{13}C] and [2, 3, 4- ^{13}C] aspartate isotopomers (Figure 3D) mirroring the deep dysfunction of the Krebs cycle. As indicated in Figure 3B, glumatate productions was further adversely effected in all the cases of the analyzed isotopomers visible in NMR spectra. Given that amino acids such as are glutamate and aspartate are particularly important for growth and proliferation, this level of deep down regulation of their synthesis might cause growth retardation but, in our opinion shall not cause lethality. Thus we presumed, that MAF1 deficient cells redistribute carbon flux away from TCA at permissive and elevated temperature and we were interested in the detailed dissection of the flux rewiring.

Preprints (www.preprints.org) | NOT PEER-REVIEWED | Posted: 26 July 2023 doi:10.20944/preprints202307.1751.v1

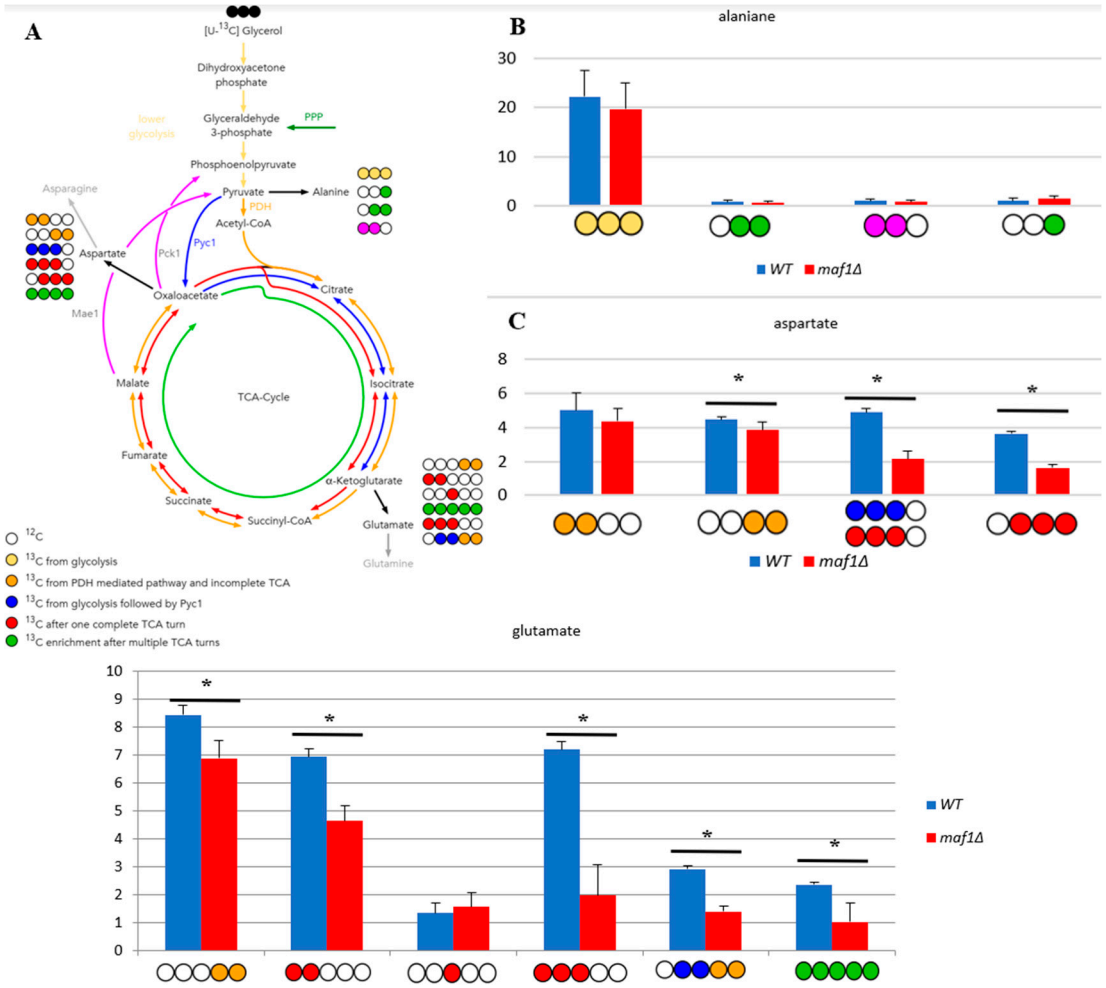

Figure 3. Lowered TCA activity under non-permissive conditions in MAF1 knockout strain. Comparative analysis of ^{13}C-labelling in alanine (B), aspartate (C) and glutamate (D) isotopomers. Yeast cells were grown in rich medium (YP) supplemented with 2 % [U-^{13}C] glycerol (YPGly) (B, C, D) until log phase. Additionally, cells were incubated for 1 h at 37°C (B,C, D). Cultures were grown overnight in YPGly (B, C, D) medium. Zero stands for the incorporation of 12C and 1 indicates ^{13}C-labelling. Data are shown as mean percentage amino acids mass isotopomer distribution with standard deviation (SD) from three independent biological replicates. As a simplification, the unlabeled (0 0 0) amino acid fractions were omitted from the graph. (A) Schematic simplified diagram of the possible incorporation of ^{13}C atoms from [U-^{13}C] glycerol to isotopomers of aspartate and glutamate. Carbon atoms are shown as circles. Filled circles represent ^{13}C and empty circles – ^{12}C atoms. Blue circle represents labelling derived from glycolytic pyruvate followed by cataplerotic reaction mediated by Pck1 into TCA. Deep yellow circle shows ^{13}C obtained from acetyl-CoA formed from glycolytic pyruvate by pyruvate dehydrogenase complex (PDH) and exit the TCA before completion of one full cycle. Red circle symbolizes the atom that left Krebs cycle after at least one complete turn. Stripped red circle represents ^{13}C enrichment that achieved at least two full cycles of TCA before redirection of the carbon flow into biosynthesis pathways. Colorful arrows symbolize the carbon flow that has led to specific labelling positions. Asterisk (*) indicates p value ≤ 0.05 by Student's t test.

2.4. Malic enzyme is the key enzyme responsible for cataplerosis in maf1Δ effecting the mutant viability.

Intriguingly, high abundance of PDH derived [1,2-^{13}C] aspartate isotopomer in *maf1Δ* during oxidative metabolism, was a reason to investigate on TCA cycle enzymes activities. As presented in Figure 1A, aspartate can be formed via a route, in which cataplerotic reaction mediated by malic enzyme (Mae1) would convert the citric acid cycle intermediates, [1,2-^{13}C] malate to into [1,2-^{13}C] pyruvate and that recycled via PDH and acetyl-CoA into [1,2-^{13}C] oxaloacetate. (Figure 1A,C). In

Preprints (www.preprints.org) | NOT PEER-REVIEWED | Posted: 26 July 2023 doi:10.20944/preprints202307.1751.v1

this case, carbon flow through the Pck1-mediated pathway is unlikely contributor, because [1,2 ^{13}C] phosphoenolpyruvate, formed from [1,2-^{13}C] oxaloacetate, would drain away into gluconeogenesis. The PDH-based recycle hypothesis has been also indicated by our computer simulations. With computer simulations in custom delta maf1FBA model we were able to reproduce experimental observations and partially elucidate metabolic activity influenced by this important mutation. MAF1 knockout in silico was created by removing reactions, which are activated by Maf1 [13,16] (Table S2). Computer simulations employed Constraint-based Modelling in Surrey Flux Balance Analysis software (Surrey FBA) shown increased flux via E1 alpha subunit Pda1 of the pyruvate dehydrogenase (PDH) complex, in *maf1Δ* strain model *in silico* (Table S3).

In order to verify our hypothesis and support further our observations, we supplemented the ^{13}C flux data by additional experimental data measuring several TCA enzymes activities. Pck1 has been the major suspect of flux rewiring in TCA in *maf1Δ* at non-permissive temperature. However as showed in Figure 4A, Pck1 enzymatic activity is decreased in *maf1Δ,* temperature shift does not influence Pck1 activity in *maf1Δ* in non-fermentable carbon source. The direct cause of flux redirection away from gluconeogenesis seems NADP+ dependent malic enzyme supported by malate dehydrogenase (Mdh1), since *maf1Δ,* exhibits reduction of Mdh1 activity regardless carbon source (Figure 4C).

Malic enzyme (Mae1) assay, shown upregulated activity in *maf1Δ* as well in *rpc128-1007* on non-fermentable carbon source both at 30°C and 37°C (Figure 4B). No significant changes were observed for Mae1 Vmax under fermentative conditions. Consequently, obtained results does not fully support the hypothesis of Pck1 enzymatic activity in TCA flux redistribution, but may indeed serve as additional constrain resulting in the observed flux redirection towards aspartate, mainly due to elevated carbon flux through Mae1 mediated shunt replenishing TCA from malate and producing pyruvate from TCA incomplete cycle in *maf1Δ* (as a futile cycle).

Malate dehydrogenase (Mdh1) uses malate as substrate and might compete for the substrate with Mae1. Mdh1converts malate to oxaloacetate, however when less active, produces less substrate for Pck1 catalysed reaction.

According to our data, Mdh1 appears as another key constrain in flux redirection towards pyruvate instead of phosphoenolopyruvate in MAF1 gene deleted strain, as we found, that Mdh1 activity is significantly decreased in *maf1Δ,* when cells were grown in glycerol (Figure 4C). This result is consistent with the overall down regulation of TCA cycle in the mutant with high RNAP III activity. In contrast, a positive co-relationship between Mdh1 high activity and TCA overall activity based on ^{13}C flux analysis, can be noted on glycerol based medium in *rpc128-1007* (Figure 4C).

Preprints (www.preprints.org) | NOT PEER-REVIEWED | Posted: 26 July 2023 doi:10.20944/preprints202307.1751.v1

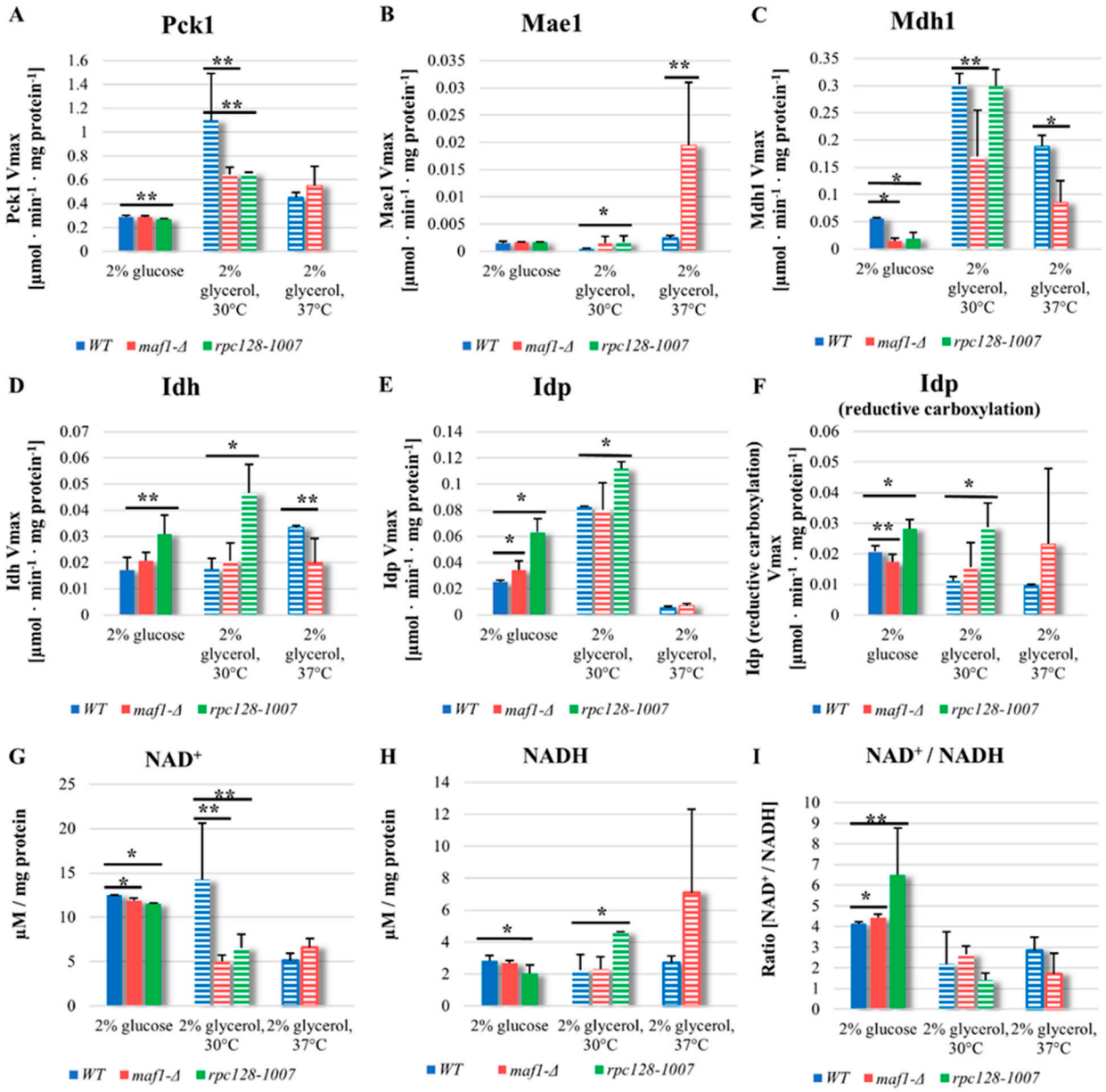

Figure 4. Under non permissive conditions, Mae1 is a key enzyme responsible for cataplerosis in *maf1Δ*. Idp dependent reductive carboxylation of glutamine is proposed as an alternative metabolic strategy in rpc128 1007, to maintain viability on glucose medium. Yeast cells were grown in rich medium (YP) supplemented with either 2 % glucose or 2 % glycerol at 30°C. To verify the phenotypic effect of MAF1 deletion, cells grown in YPGly were transferred for 2 h to 37°C. All enzymatic activities were measured in cell-free yeast extracts (A, B, C, D, E, F). The reaction rates were monitored by measuring NADH concentration change over time at 340 nm. Protein concentration was assessed according to Bradford assay. Data are expressed as the mean Vmax obtained from at least three independent biological replicates. NAD+ and NADH levels were measured according to NAD/NADH Assay Kit II (colorimetric, ab221821, Abcam) as stated in manufacturer's protocol (G, H, I). NAD+ and NADH concentrations expressed in µM was calculated from standard curve and standardized to total proteins concentration expressed in mg. The + standard deviations (SD) are shown. Asterisk (*) indicates p value ≤ 0.05 and double asterisk (**) mark p values ≤ 0.1 by Student's t test.

Preprints (www.preprints.org) | NOT PEER-REVIEWED | Posted: 26 July 2023 doi:10.20944/preprints202307.1751.v1

2.5. Reductive carboxylation of glutamine is the survival strategy of rpc128-1007 grown on glucose.

Despite the decreased glycolytic activity, the *rpc128-1007* strain is still able to growth on fermentable carbon source, although shows grow rate reduction [13]. This has been a puzzling observation to us requiring further investigation. In theory, when glycolysis is blocked, reductive carboxylation of glutamine may serve as an alternative source for metabolic intermediates [20] where citrate is formed from α-ketoglutarate (AKG) by isocitrate dehydrogenase (Idh or Idp). To determine whether reductive carboxylation of α-ketoglutarate to D-isocitrate is occurring in rpc128 1007, enzymatic activity of NAD+ dependent isocitrate dehydrogenase Idh1-3 and NADP specific isocitrate dehydrogenase Idp1-3 were measured in both directions, conversion of D-isocitrate to AKG and AKG to D-isocitrate (reduction carboxylation reaction).

We found that the activity of both, Idh1-3 and Idp1-3, are upregulated in *rpc128-1007* regardless the carbon source (Figure 4D). No activity in reduction carboxylation, that might be Idh1-3 dependent, was noted for none of the tested strains in our assays (data not shown). Consistent with the working hypothesis, there is a significant increase in Idp1-3 activity in reductive carboxylation direction in *rpc128-1007* regardless the carbon source.

The intracellular redox potential is primarily determined by the NADH/NAD+ ratio and to a lesser extent by the NADPH/NADP+ ratio [21]. It has been shown by other authors that the reductive carboxylation of glutamine can be induced by unbalanced cellular ratio of NAD+ to NADH [22]. Maintenance of NAD/NADH ratio is essential for mitochondrial function, therefore, we determined the ratio in the mutant strains. Firstly, as shown in the Figure 4I, both strains with altered RNAP III activity have elevated level NAD+/NADH ratio. Increased NAD+/NADH ratio in the cytoplasm has been reported as a hallmark of efficient glycolysis that would be true for *maf1Δ*, the strain with high glycolytic activity [23]. In the case of *rpc128-1007*, which is unable to utilise glucose efficiently via glycolysis, presented data strongly support the hypothesis of reductive carboxylation of glutamine as a survival metabolic strategy of *rpc128-1007*. On the other hand, under non-fermentable growth conditions, increased NADH level is observed in *rpc128-1007*, supporting the view of increased efficiency of TCA cycle in this strain as presented in Figure 4H. (the middle bars set).

The NAD+/NADH ratio in Maf1 deficient cells, seems to be perturbed under glycerol growth conditions at 37°C. We presume that the activity of PDH complex might contribute to the observed increase in NADH concentration in this mutant cells.

2.6. maf1Δ and rpc128-1007 show enhanced acetyl-CoA and lipids content.

Finally, to support the putative increase in activity of PDH, we measured the level of cellular acetyl-CoA, as this metabolite is an intermediate link between glycolysis and TCA cycle. Since measuring the concentration of acetyl-CoA in various cellular compartments, seems technically not trivial, many authors interpret the total level of this metabolite as an indicator of nucleo-cytosolic pool of the compound in the cell [24,25].

To extract acetyl-CoA, the yeast cultures were grown in YPD or YPGly at 30°C. Additionally, half of the cultures grown in YPGly was shifted from 30°C to 37°C for 2 h. The acetyl-CoA was extracted and measured according to MAK039-1KT fluorometric kit (Sigma Aldrich).

As indicated in Figure 5, in yeast the level of acetyl-CoA under glucose conditions is higher than on non-fermentable carbon source, which was also reported before for wild type cells [24]. Surprisingly, in both mutated strains, acetyl CoA concentration is approx. 2-fold higher compared to WT (Figure 5A), when cells are in the log growth phase. The result obtained for *maf1Δ* can be explained by increased activity of glycolysis [13], but the accumulation of acetyl-CoA in *rpc128-1007* seems unusual. Additionally, accumulation of acetyl-CoA in *maf1Δ* can be supported by deficiency of glyoxylate shunt revealed previously by proteomic data [13], which consumes acetyl-CoA to produce malate. The total cellular acetyl-CoA level measured in the strains with altered RNAP III under respiratory conditions is decreased (Figure 5A).

Preprints (www.preprints.org) | NOT PEER-REVIEWED | Posted: 26 July 2023 doi:10.20944/preprints202307.1751.v1

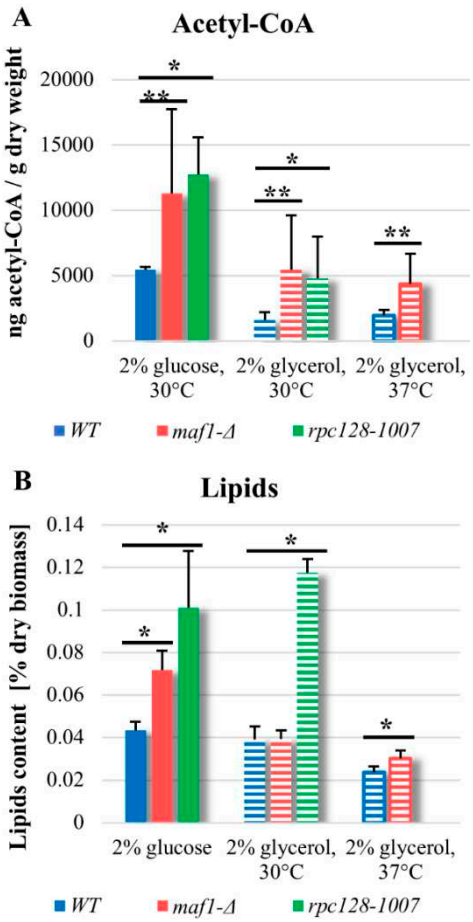

Figure 5. Acetyl-CoA concentration is higher in logarithmically growing yeast cells with altered RNAP III activity (A), which is consistent with lipids content on glucose (B). Yeast cultures were grown in YPD or YPGly medium until OD600 ≈ 1.0 at 30°C. For WT and *maf1Δ* cells that were grown in glycerol-based medium, additional 2 h long incubation at elevated (37°C) temperature was done. For acetyl CoA measurement (A), yeast cells metabolism was rapidly stopped by quenching in cold HPLC-grade methanol (-80°C). Acetyl-CoA extraction was performed as was described in Materials and Methods. Acetyl-CoA concentration was measured using Acetyl-Coenzyme an Assay Kit (MAK039-1KT, Sigma Aldrich). The extraction of total cellular lipids (B) was done from the lyophilized biomass with chloroform:methanol mixture (2:1, v/v). Lipids were recovered by evaporation of the bottom layer solvent and pellets weighted. The obtained result is percentage of lipids content in cell dry weight. All results are shown as mean value from at least three independent biological replicates with standard deviations (SD). Asterisk (*) indicates p-value ≤ 0.05 and double asterisk (**) mark p-values ≤ 0.1 by Student's t-test.

Acetyl-CoA is a precursor for synthesis of lipids. There are several studies from Maf1 deficient model organisms, including *C. elegance*, *S. cerevisiae* and human cells, [26–28] which show that deletion of MAF1 gene results in accumulation of fatty acids or lipids. No published data exist so far indicating that it occurs in *maf1Δ* cells or in cells with compromised RNAP III, that are capable of such accumulation when grown on non-fermentable carbon source. Therefore, next step in our investigation was, determination of the concentration of lipids in the mutated strains in glucose-based and glycerol-based medium.

Lipids content measured in *maf1Δ* and *rpc128-1007* (Figure 5B), under fermentative growth conditions is corelated with elevated concentration of acetyl-CoA, respectively in both the strains, and it is increased when compared to the control. Higher concentration of acetyl-CoA as well lipids, can be observed also in *rpc128-1007* grown under respiratory conditions and in *maf1Δ* after a shift to 37°C (Figure 5B). Despite the increased concentration of acetyl-CoA in *maf1Δ* grown on glycerol-based

 doi:10.20944/preprints202307.1751.v1

medium, the content of lipids per g dry weight does not seem to be significantly higher. Lipids droplets are the major reservoir for lipids in *maf1Δ* grown on glucose and on glycerol at restrictive temperature. To conclude, it seems not the case for *rpc128-1007* as indicated by microscopy investigation and might be a manifestation of significant changes in lipid composition of cell membranes (Figure S1).

3. Discussion

Mitochondrial dysfunction has been associated with major civilization diseases including type 2 diabetes, Alzheimer's diseases and several other neurodegenerative disorders therefore accelerated health problems at aging [19,29]. The molecular basis of disease is different and involves different levels of regulation of cellular activity. Due to systems biology approaches applied in basic research, we are closer than ever to answer the fundamental question, how metabolic incapability is correlated with non-coding gene regulation to understand the health or disease related physiology at cellular level.

In the case of RNAP III compromised strain (*rpc1128-1007*) with phenotypic growth defect on glucose we previously successfully explained its growth defect on glucose at the level of enzymes activities and enzymes abundance [13]. We also established a new metabolic link between mitochondrial proteome abundance and RNAPIII driven non-coding RNA synthesis. Further under the course of this study, we intended to characterize mitochondrial activity in depth to address a few urgent questions related to the mutants phenotypes dependent on carbon source and lethality at higher temperature.

The focus of our current report was to investigate the possible impact, RNAP III activity exerts on mitochondrial metabolism and carbon flux distribution in TCA cycle under different growth conditions. Our previously reported observations related to mitochondrial proteome in the mutant strains with non-optimal RNAP III activity (*rpc128-1007* and *maf1Δ)* highlighted a possible scenario for alterations in the mitochondrial metabolism that required further investigation at metabolic level to allow for drawing a final conclusion on its activity.

By this study we shown, that RNA polymerase III overactivity as well as its downregulation can adversely affect TCA flux via TCA enzymes activities in *S.cerevisiae* when RNAP III activity is not optimal for appropriate grown conditions. Compromised RNAPIII activity seems to lower mitochondrial TCA activity when compared to the wide type cells, if glucose is abundant, but the C128 mutation can be also beneficial when poor source of carbon, such as glycerol is the only option for the uptake of carbon source.

We recognize the potential of precise optimization of RNAP III activity towards balancing aberrant mitochondrial metabolism by the manipulation of the holoenzyme activity, but not by its full inhibition. In our opinion, non-optimal RNA production driven by RNAPIII, is a superior signal over the extracellular glucose signaling in *S.cerevisiae*, which observation we reported previously [12].

Non-optimal RNA synthesis is followed by systemic metabolic adjustment of mutant cells and causes the cells lack of plasticity at adopting either to fermentable or non-fermentable carbon, thus mimics metabolic disorder hallmarked by unidirectional metabolism of cancerous cells and cells depraved from nutrition.

3.1. RNAP III non-optimal activity affects the TCA flux and TCA enzymes activities.

It is believed that yeast cells lower the level of TCA cycle activity, the flux on glucose regardless of oxygen availability [30,31]. The generally held view of a catabolite repressed TCA cycle in glucose-excess cultures of *S.cerevisiae* contrast with Blank and Sauer observation, that although the TCA cycle genes are subject to glucose repression [32] the relative respiratory activity of the TCA cycle may increase even at high glucose concentration provided the growth rate or the glucose uptake are impaired [33]. Our data supports the view represented by Blank and Sauer, claiming that the regulation of TCA cycle activity is not under transcriptional control of the genes, that are subject to glucose repression. In contrast to Blank and Sauer observation done on TCA cycle activity in CEN.PK113-7D genetic background, we do not observe increased TCA cycle activity in *rpc128-1007* strain with the

Preprints (www.preprints.org) | NOT PEER-REVIEWED | Posted: 26 July 2023 doi:10.20944/preprints202307.1751.v1

compromised RNAP III activity (Figure 6B). Cells with compromised RNAP III (*rpc128-1007*) grown in glucose, show increased transcription of high affinity glucose transporters HXTs, reduce concomitantly their growth and uptake of glucose with no increase in TCA cycle activity on glucose (Figure 1G) [12,13]. This suggest that other factors than growth rate or glucose uptake determine the TCA cycle activity in *S.cerevisiae*, undoubtedly an intracellular factor.

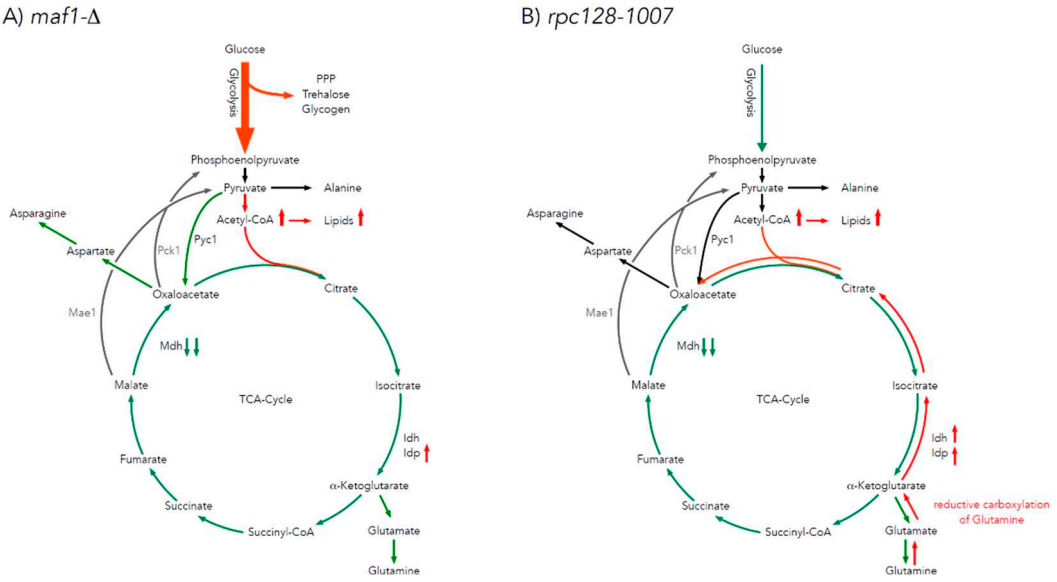

Figure 6. Model of carbon flow through TCA cycle in MAF1 deletion and *rpc128-1007* mutants grown on glucose. During fermentative growth on glucose, MAF1 knockout strain exhibits accelerated glycolysis (A) compared to WT [13]. Glucose flux is redirected into PPP, trehalose, glycogen, and glycerol biosynthesis (18) and acetyl-CoA and lipids formation (Figure 5). TCA cycle activity is slightly diminished in MAF1 knockout strain due to carbon drained towards glutamate biosynthesis (Figures 1F). While growth on glucose, *rpc128-1007* (B) mutant shows downregulated glycolytic activity [13] in comparison to reference isogenic strain. Also, citric acid cycle activity is lowered (Figure 1G). TCA is supported by Pyc1 mediated rout and Idp dependent reductive carboxylation of glutamine, which results in elevated acetyl-CoA pool to support lipids biosynthesis. Green represents a diminished carbon flux and pink represents an elevated flux compared to WT. Abbreviations: TCA – citric acid cycle, PEP – phosphoenolpyruvate, PYR – pyruvate, OAA - oxaloacetic acid, CIT – citrate, ICI – isocitrate, AKG – α ketoglutarate, SUC – succinate, FUM – fumarate, MAL – malate, Ala – alanine, Gln – glutamine, Glu – glutamate, Asp – aspartate, Asn – asparagine, PPP – pentose phosphate pathway, Pck1 - phosphoenolpyruvate carboxykinase 1, Mae1 - malic enzyme 1, Mdh - malate dehydrogenase, Idh - NAD+-specific isocitrate dehydrogenase, Idp - NADP-specific isocitrate dehydrogenase.

The broad change in the abundance profile of enzymes engaged in TCA seems to affect the *maf1Δ* TCA activity rather lesser when compared to its suppressor (*rpc128-1007*) (this study). This suggests that the control of TCA cycle activity is not enzymes abundance dependent. Other factors (metabolites, non-coding tRNAs) can be in place [34]. In yeast strains with altered RNAP III activity (*maf1Δ* and *rpc128-1007*), the carbon flux through the citric acid cycle is diminished more than in the reference strain under high glucose conditions (Figure 6A,B). The low percentages participation of [2, 3- ^{13}C] aspartate, [1,2- ^{13}C], [3- ^{13}C], [4,5- ^{13}C], -glutamate isotopomers (Figure 1E,G, Table A1), suggests that the carbon pool in the TCA cycle is replenished not only towards biosynthesis of glutamate, but also redirected towards different metabolic routes unlike in the wild-type strain. The change in TCA activity is reflected rather by flux direction. Glutamate is synthesized in cell with compromised RNAPIII via Pyc1 shunt, when in Maf1 deficient mutant, isotopomers of glutamate are more efficiently formed *via* PDH mediated pathway (Figures 1F and 6B).

Additionally, under this investigation, higher concentration of nucleocytosolic pool of acetyl-CoA was confirmed for *maf1Δ* (Figure 5A). The distribution of pyruvate-derived alanine isotopomers in *maf1Δ* does not show an increased concentration of the end-point glycolytic metabolite, pyruvate.

 doi:10.20944/preprints202307.1751.v1

However, except for alanine biosynthesis, pyruvate can be converted into ethanol or acetyl-CoA. No increase in ethanol synthesis was observed in *maf1Δ* [13]. Therefore, the high levels of acetyl-CoA (Figure 5A) found in *maf1Δ* point at pyruvate, as an abundant metabolic source channeled into acetyl-CoA. The increase in acetyl-CoA concentration guides cellular metabolism towards biosynthesis processes, e. g. by transcriptional mechanism, and shuts off catabolic reactions [35]. This effect of redirecting metabolism towards anabolic reactions, when the level of acetyl-CoA is elevated in *maf1Δ* is supported by, observations of accumulation of lipid in lipids droplets (Figure S1). Accordingly, to several studies on model organisms including *C. elegance*, mammalian cells and *S. cerevisiae* [26–28,36] Maf1 negatively regulates lipid metabolism. Consequently, we assume that increased accumulation of acetyl-CoA and lipids in *maf1Δ* is a result of an increased uptake of glucose and increased activity of PDH complex, suggested by modelling.

Despite low glycolytic activity observed in *rpc128-1007*, high concentration of acetyl-CoA and lipids (Figure 5B) can be accumulated also in *rpc128-1007*. The collected data implies, that reductive carboxylation is the potential source of cytosolic acetyl-CoA in *rpc128-1007* (Figure 6B). We confirmed that enzymatic activity of both isocitrate dehydrogenases, NAD+-specific Idh and NADP-specific Idp, are upregulated in the mutant strain grown on glucose (Figure 4D,E). Idp, but not Idh, has also increased activity in reductive carboxylation reaction (Figure 4F). Therefore, we favor the scenario, that reductive carboxylation of glutamine in *rpc128-1007* depends on Idp cellular activity.

Reductive carboxylation of glutamine is an alternative metabolic pathway, where citrate synthesis occurs by a reductive carboxylation of α-ketoglutarate (AKG) catalyzed by isocitrate dehydrogenase (Idh or Idp) at the expense of citrate formation in the pyruvate decarboxylation reaction. Cells utilize glutamine to sustain TCA cataplerosis, nucleotides and fatty acids biosynthesis, as well the redox balance [37]. Glutamine is utilized at a high rate by rapidly growing cells. For instance, glioblastoma cells have upregulated aerobic glycolysis as well as active TCA with a strong carbon efflux into fatty acids biosynthesis pathways. These cells exhibit a very high catabolism of glutamine, which is a source of the carbon backbone for TCA replenishment. Therefore, citrate generated by reductive carboxylation may be used for lipid biosynthesis in the cells [38]. Reductive metabolism of glutamine or glutamate for lipid biosynthesis allows cells to save the glucose-derived carbon for production of biosynthetic precursors like ribose, that is not usually synthetized via other routes [39]. Glutamine is a carbon backbone source for biosynthesis of lipids and acetyl CoA was previously reported for a brown adipocyte cell line [40] and A549 cells growing under hypoxia [39].

The concentration of NAD+ and NADH measured in *rpc128-1007* grown on glucose is decreased compared to the wild type. Even though, we see a significant increased NAD+ to NADH ratio in this mutant strain (Figure 4I). In our opinion the change in the NAD+ to NADH cell ratio supports lipid biosynthesis possibly because of impaired utilization of NADH by the mitochondrial respiratory chain induced by reductive glutamine carboxylation [22]. This redox imbalance further suggest that mitochondrial respiratory chain might be dysfunctional in the *rpc128-1007* strain grown on glucose.

Here we depict first, that accumulation of lipids can be observed in *rpc128-1007* strain in high glucose medium. Therefore we presume, that synthesis of different classes of RNA and their abundance might be an intracellular signal stimulating lipids accumulation of different classes of lipids, for instance lipids building the *S.cerevisiae*, membranes, not necessarily involving formation of lipids droplets.

It is likely, that changes in the content of lipids in yeast strains with different tRNA levels is connected to tRNA metabolism or lipids modification. Except of the role of aminoacyl transfer RNAs (aa tRNA) in translation, the transfer RNAs in bacteria were shown to participate in membrane lipid aminoacylation [41]. *in vitro* study on tRNAs has showed association of yeast tRNA with phospholipid bilayers [42]. More recent research has showed that lipids can protect RNA and modulate ribozyme activity via RNA-lipid interactions [43].

To conclude, the perturbed activity of RNAP III indirectly reduces TCA activity during fermentative growth. Both mutant strains accumulate lipids and its precursor acetyl-CoA. By contrast, different routes lead to the observed increased in lipids accumulation, in *maf1Δ* in *rpc128-1007* (Figure 6A,B).

Preprints (www.preprints.org) | NOT PEER-REVIEWED | Posted: 26 July 2023 doi:10.20944/preprints202307.1751.v1

3.2. The difference in growth of the mutants with altered RNAP III activity on a non-fermentable carbon source results from flux rerouting

As indicated by our study, the metabolic strategy, that helps yeast cells with comprised RNAP III activity (*rpc128-1007*) to metabolize glycerol efficiently and to partially overcome growth retardation on glucose, it is primarily flux redirection. Therefore, the mutant depraved from Maf1 when crossed with *rpc128-10007* is able to adjust its grown towards more efficient metabolism of non-fermentable type of carbon source.

As hypothesized, the study of *maf1Δ* and its suppressor by ^{13}C flux analysis in the presence of uniformly labelled glycerol, showed that, unlike *maf1Δ*, its suppressor displayed high TCA activity (Figures 2A and 7A,B). In *maf1Δ*, downregulation of complete TCA cycle is observed deducted from the splitting of ^{13}C carbon in the percentage fraction of [2,3,4 ^{13}C] aspartate derived from one complete TCA, formation of [1,2 ^{13}C] aspartate and [3,4 ^{13}C] aspartate as a result of incomplete TCA cycle (Figure 2C). The increase in [1,2 ^{13}C] aspartate pool concomitantly observed with highly pronounced reduction of flux towards glutamate biosynthesis in response to glycerol-based medium (Figure 2D), suggests that TCA cycle operates as a bifurcated pathway to sustain biomass precursors (aspartate) requirement. In this case, in *maf1Δ*, TCA cycle would not operate as a cycle, but rather two-branched-pathway, similarly to batch-growing cells, and in contrast to the chemostat condition [44]. The synthesis of aspartate can be additionally supported by glutaminolysis, which takes place in all proliferating cells [45].

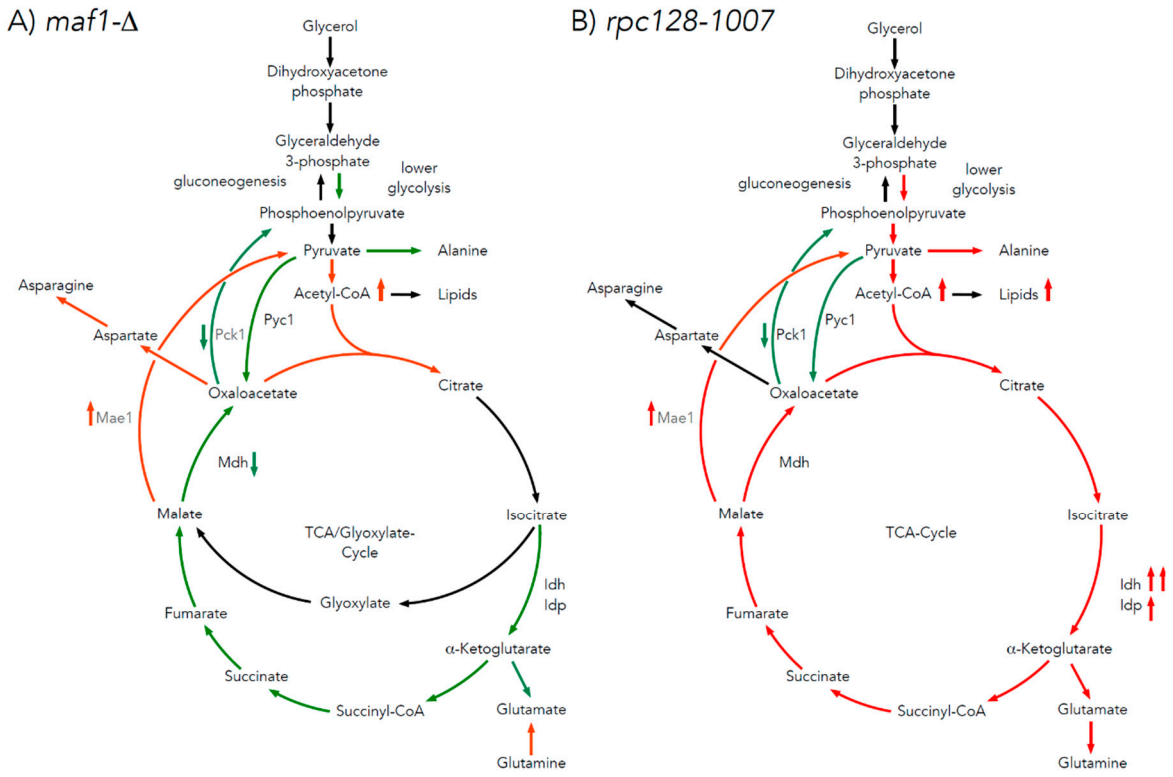

Figure 7. Proposed model of carbon flow through TCA cycle in MAF1 deletion and rpc128 1007 mutants grown on glycerol**.** On non-fermentable carbon source, yeast strains with changed RNAP III exhibit contrary metabolic adjustments. MAF1 deletion strain shows diminished lower glycolysis, pentose phosphate pathway (PPP), TCA including anaplerotic pathways (A). TCA is additionally replenished by highly active Mae1 mediated pathway. Acetyl CoA level is higher (Figure 5A) than in the wild type (A), which does not correlate with lipids levels. Meanwhile, rpc128 1007 has highly active lower glycolysis and TCA cycle (B), including acetyl-CoA and lipids accumulation (Figure5B) and reaction directed by PDH. Yet, Pyc1-mediated anaplerotic pathway seem to be less active than in the reference strain. Malate is directed towards pyruvate by Mae1 mediated reaction, rather than Asp biosynthesis pathway (B). Green represents diminished carbon flux, while red stands for elevated

 doi:10.20944/preprints202307.1751.v1

flux, when compared to WT. Abbreviations: TCA – citric acid cycle, PEP – phosphoenolpyruvate, PYR – pyruvate, OAA - oxaloacetic acid, CIT – citrate, ICI – isocitrate, AKG – α ketoglutarate, SUC – succinate, FUM – fumarate, MAL – malate, Ala – alanine, Gln – glutamine, Glu – glutamate, Asp – aspartate, Pck1 - phosphoenolpyruvate carboxykinase 1, Mae1 - malic enzyme 1, Mdh - malate dehydrogenase, Idh - NAD+-specific isocitrate dehydrogenase, Idp - NADP-specific isocitrate dehydrogenase.

The low percentages participation of [3,4- ^{13}C] and [1,2,3- ^{13}C]-aspartate as well as all the detected isotopomeric forms of labelled glutamate in *maf1Δ* after temperature shift (Figure 3C,D, Table S1), suggests that the carbon pool in the TCA cycle is replenished not only towards biosynthesis of glutamate, but also towards aspartate unlike in the *maf1Δ* at permissive temperature.

On a glycerol based medium, both *maf1Δ* and *rpc128-1007* strains show increased levels of acetyl-CoA (Figure 5A). Since acetyl-CoA activates Pyc1, the reduced carbon flux through the Pyc1 driven pathway can be explained either by high amino acid abundance provided by TCA (the most probable for *rpc128-1007*) or by higher pyruvate pool (suggested for *maf1Δ).*

Under respiratory conditions, the pyruvate fraction can be supplied by cataplerotic pathways involving activity of phosphoenolpyruvate carboxykinase 1 (Pck1) and malic enzyme 1 (Mae1). We are showing here that Pck1 enzymatic activity is lowered in *maf1Δ* equally in its suppressor strain *rpc128-1007*, while Mae1 activity is higher in both mutants at high non-fermentable carbon source concentration (Figure 4B). Further the downregulation of Mhd1 activity (Figure 4C) and significant increase in Mae1 in *maf1Δ* on glycerol after shift to 37^{o}C contributes to flux directing towards pyruvate and fuels acetyl-CoA biosynthesis (Figure 8). We demonstrate increased lipid biosynthesis in *maf1Δ* strain, after temperature shift of glycerol growing *maf1Δ* culture to 37^{o}C (Figure A1).

Mae1 is a major participant in lipids biosynthesis therefore it has a contribution in development of obesity and type 2 diabetes [46]. It contributes to the NADPH pool and is engaged in buffering of ROS via NADPH-dependent recycling of glutathione/ thioredoxin pathways, working in concert with other NADP-recycling cytosolic enzymes G6PD, PGD, IDH1 and MTHFD [47,48]. The biosynthesis of membrane components such as fatty acids and cholesterol and the pyruvate-malate cycle, provide essential support for cancer cell proliferation and migration in Mae1 dependent cancer cells metabolism [49]. It is worth investigating, under which circumstances a significant increase in Mae1 activity, that is pro-oncogenic enzyme in diverse tissues, accompanied by inhibition of Mdh in proliferation cell line can cause lethality.

Preprints (www.preprints.org) | NOT PEER-REVIEWED | Posted: 26 July 2023 doi:10.20944/preprints202307.1751.v1

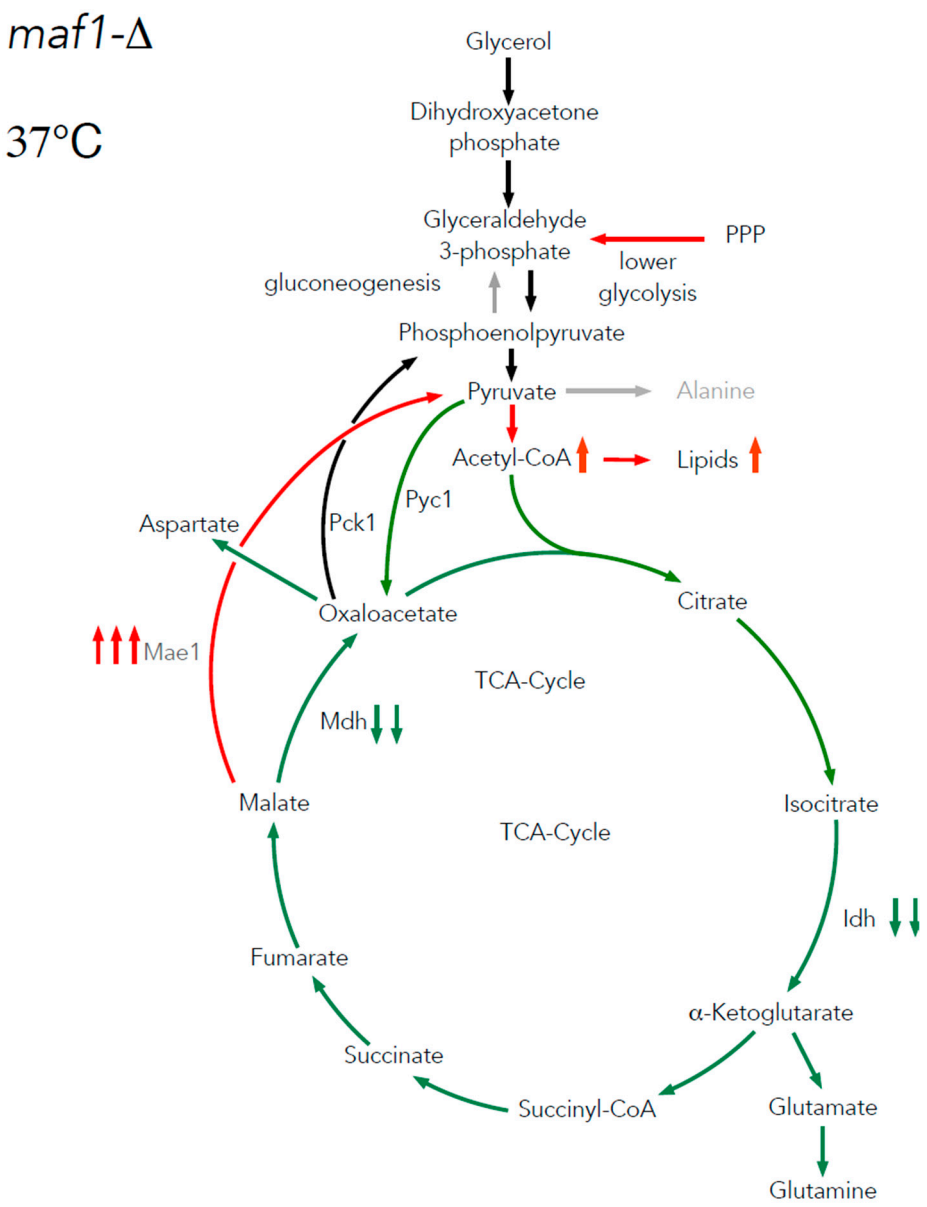

Figure 8. Proposed model of carbon flux through TCA during growth arrest of *maf1Δ* cells under non-permissive conditions. Gluconeogenetic flux is redirected into the Mae1-catalysed pathway. Down-regulation of FBP1 (54) prevents further gluconeogenesis from occurring, so the carbon flow is directed towards pyruvate, acetyl-CoA and lipids biosynthesis. Green colour represents lowered carbon flux, while red stands for enhanced activity of the pathway. Abbreviations: TCA – citric acid cycle, PEP – phosphoenolpyruvate, PYR – pyruvate, OAA - oxaloacetic acid, CIT – citrate, ICI – isocitrate, AKG – α ketoglutarate, SUC – succinate, FUM – fumarate, MAL – malate, Ala – alanine, Glu – glutamate, Asp – aspartate, Pck1 - phosphoenolpyruvate carboxykinase 1, Mae1 - malic enzyme 1, Mdh - malate dehydrogenase, Idh - NAD+-specific isocitrate dehydrogenase, Idp - NADP-specific isocitrate dehydrogenase.

Analysis of the liver of MAF1 knockout mice (which is metabolically similar to yeast cells grown on non-fermentable carbon source) by metabolomic profiling, showed that most of glycolytic and TCA intermediates were not affected by the deletion, with the exception of pyruvate and acetyl CoA, which levels were diminished [2]. This is in contrary to the observations in *maf1Δ* cells presented in this work (Figure 5A). Contradictory to findings presented here, in the KO mice liver enhanced carbon flux through TCA cycle was observed [2]. This may indicate that although the alteration in RNAP III activity affects carbon metabolism in eukaryotes, the endpoint metabolic effects may be species dependent. With the exception to the contradictory observation in acetyl-CoA levels in the Maf1

 doi:10.20944/preprints202307.1751.v1

deficient models (the single cell yeast and vertebrate), KO mice metabolism shows similarity to *rpc128-1007* metabolism, therefore alternative hypothesis exists, that KO mice might enquired compensating mutations.

Since our data in *S.cerevisiae* cells are partially contesting the published data on mitochondrial metabolism in KO mice maf1+/-, we think it is worth reinspecting the metabolism using other, well studied eukaryotic model organisms, to answer the question whether lack of Maf1 protein corelates with dysfunction of mitochondrial metabolism and obesity or tumorigenesis.

4. Conclusions

Taking into an account the importance of mitochondrial activity to cellular metabolism, redox state, ATP production, genome stability thus longevity regulation [50] our ^{13}C flux comprehensive data on cells representing non-optimal RNAP III activity (*maf1Δ* and *rpc128-1007*), provides new valuable insights into possible perturbation caused by the non-optimal, non-coding RNA biosynthesis process to the cell's metabolism [13]. This bring both, detrimental consequences, which can be phenotypically observed as a growth arrest, as well as hidden metabolic changes, which in the case of unicellular eukaryotic organism such as *S.cerevisiae*, can be easily followed utilizing methods such as ^{13}C flux analysis. Global metabolomics data are still difficult to interpret, for instance when performed under semi-controlled nutritional conditions. Therefore, we believe, that the ^{13}C flux data presented here and obtained by direct tracking of the intracellular carbon flux distribution in a living cell are of high importance and meaningful contribution to the current state of knowledge on RNAP III global impact on metabolism of eukaryotic cells.

5. Materials and Methods

5.1. Yeast culturing and metabolites extraction for ^{13}C flux analysis by nuclear magnetic resonance (NMR) spectroscopy

Twice concentrated rich (2xYP) medium without carbon source (pH 5.0) was prepared. In addition, 100 mM potassium hydrogen phthalate (C8H5KO4) was supplemented to the medium to compensate pH fluctuations of the medium [51]. Prior culturing yeast strains [1,2-^{13}C]-glucose (453188, Sigma-Aldrich) and uniformly labelled [U-^{13}C]-glycerol (489476, Sigma-Aldrich) were suspended in Milli-Q water to a final concentration of 4% and sterilized by filtration. The 2 x YP medium was mixed with glucose or glycerol solution (1:1) to obtain 2% final concentration of ^{13}C-labelled carbon source in the medium.

Overnight yeast cultures were centrifuged and washed twice with YP medium without carbon source. Yeast cells grown overnight at 30°C (250 rpm) in YPGly were transferred to YPGly medium with [U-^{13}C]-glycerol. For determining the carbon flux on glucose, yeast cells were grown overnight in YPD. To avoid revertants, *rpc128-1007* and reference strains were grown overnight in YPGly. Next, *rpc128-1007* and WT strains were shifted to YP with [1,2-^{13}C]-labelled glucose. Yeast cultures with ^{13}C-labelled carbon source were inoculated to a maximum OD600 ≈ 0.03 [52] and grown until OD600 ≈ 1.0 at 30°C, 250 rpm. Half volume of the WT and *maf1Δ* cultures grown on non-fermentable carbon source were shifted for 1 h to 37°C in order to verify the metabolic effect of MAF1 deletion. 5 ml of culture was rapidly quenched in 25 ml HPLC-grade methanol (−80°C, 34860, Sigma-Aldrich) and centrifuged for 10 min (10,000 rpm, −20°C). Pellets were washed with cold (−80°C) methanol, frozen in liquid nitrogen (−196°C) and stored at −80°C until extraction.

For metabolites extraction, the pellets were resuspended in 500 µl of mixture (1:1) HPLC-grade methanol (−80°C): water (4°C) and homogenized with Mini-Beadbeater 24 (Biospec products) using 200 µl of glass beads (425– 600 µm; Sigma-Aldrich) in 8 bursts of 10 s each with break between the cycles for 1 min incubation on ice. Next, 500 µl chloroform (−20°C) was added. Extracts were vortexed for 2 min (4°C) and centrifuged for 30 min, 13,000 rpm (4°C). The upper, polar phase was transferred into 2 ml tubes. The samples were frozen in liquid nitrogen (−196°C) and freeze-dried in Alpha 1– 2 LD lyophilizator (Christ, Chair of Analytical Chemistry).

Preprints (www.preprints.org) | NOT PEER-REVIEWED | Posted: 26 July 2023 doi:10.20944/preprints202307.1751.v1

5.2. NMR spectroscopy

The extracted and dried samples were dissolved in 120 µl of NMR buffer (100 mM sodium phosphate buffer pH 7.0, 0.2 mM SDS, 8 mM imidazole, 0.03 % sodium aside and 7.14 % deuterium water D2O). 35 µl of samples were then transferred into 1.7 mm NMR tubes using a Gilson robot. Samples were sonicated for 10 min.

All NMR spectra were acquired on an Avance III Bruker 600 MHz (14.1 T) NMR spectrometer equipped with 1.7 mm TCI cryoprobe. Spectra were acquired at a temperature of 300 K. Samples were stored at 6°C in a SampleJet automatic sample changer prior to data acquisition. 1D-1H NMR spectra were acquired using a 1D-NOESY pre-saturation pulse sequence. A total of 16384 complex data points was acquired, the spectral width was set to 12 ppm, the interscan relaxation delay was set to 4s. 16 steady-state scans and 128 transients were acquired. Prior to Fourier transform, all free induction decays (FIDs) were apodised using an exponential window function with a line-broadening of 0.3 Hz, before FIDs were zero-filled to 131072 data points. After Fourier transform, all 1D-1H NMR spectra were manually phase corrected.

Ultra-high resolution 2D-^{1}H,^{13}C HSQC NMR spectra were acquired using a gradient-selected hsqc pulse sequence using the echo/anti-echo scheme for quadrature detection. 8 steady-state scans and 2 transients were acquired. 30% of 8192 complex increments were acquired (2548 complex increments) using a non-uniform sampling scheme. The spectral widths were set to 13 ppm for the 1H dimension and 160 ppm for the 13C dimension.

The 2D-1H,13C HSQC NMR spectra were reconstructed using the IRLS algorithm with 20 iterations with MDDNMR (version 2.5) [53,54] and then processed using NMRPipe (Version 9.2) [55]. Analysis of the signal multiplets in the 2D NMR spectra included quantum mechanical simulation of the NMR multiplets and isotopomer analysis and was performed by the MetaboLab software [56]. Based on ^{13}C-^{13}C J-coupling patterns, ^{13}C isotopomer distributions were calculated based on the approach described by Chong et al. [57].

5.3. Metabolism modelling

12 genome-scale models of the *S.cerevisiae* metabolic Network Publisher since 2003 according to B. Heavner, 2015 [58] have been compared. The version chosen was a consensus yeast model Yeast7.6. A perl script allowed us for transferring annotations from yeast 7.0 to yeast 7.6 model to be used in SurreyFBA environment (65). Simple procedure for locating genes was established: 1) Take gene name from YDB, 2) Find it in “Reaction” tab in “Rule” column, 3) Write reaction Ids. Delta_maf1FBA model was designed by removing reactions, which are activated by Maf1. These reactions are indispensable for gluconeogenesis and amino acids biosynthesis pathways. *maf1Δ* leads to decrease in mRNA levels of FBP1, HXT6&7, LYS9, MET2, PCK1 and accumulates glycogen, trehalose and enhances production of glycerol [13,16]. FBA and FVA analysis were performed.

5.4. NADH-linked enzymatic assays.

Yeast cultures and cells free extracts were prepared as previously described [12,13,59]. Reaction mixtures and reagents, used to start the reaction, were different for each enzyme and had the composition as described below.

NAD+-dependent isocitrate dehydrogenase (Idh1, Idh2, Idh3, EC 1.1.1.41) activity was measured in cell-free extracts according to protocol described by Lin and co-authors [60] The reaction towards α-ketoglutarate (AKG) contained 40 mM Tris-HCl pH 7.4, 0.5 mM NAD+ (N7004, Sigma Aldrich), 4 mM MgCl2. The reaction was started with an addition of 25 µl of 11 mM D isocitrate (58790, Merc), which gave 1 mM final concentration. The conversion of α ketoglutarate (AKG) to D-isocitrate in reduction carboxylation reaction contained 250 mM Tris HCl pH 7.6, 25 mM NADH (N8129, Sigma Aldrich), 5 mM MgCl2, 40 mM NaHCO3. Reaction was started with an addition of 25 µl of 11 mM α-ketoglutarate (75890, Merck), which gave 1 mM final concentration.

NADP+-specific isocitrate dehydrogenase (Idp1, Idp2, Idp3, EC 1.1.1.42) activity was measured according to Contreras-Shannon *et. al.* [61]. The assay mixture contained 40 mM NADP+ (N5755,

 doi:10.20944/preprints202307.1751.v1

Sigma-Aldrich), 50 mM potassium phosphate buffer pH 7.75, 5 mM MgCl2 and cell free extract. Reaction was started with an addition of 25 µl of 11 mM D-isocitrate (58790, Merc), to a final concentration of 1 mM. The conversion of α-ketoglutarate (AKG) to D-isocitrate in reduction carboxylation reaction by Idp1-3 was measured according to the protocol proposed by Contreras-Shannon et al. (68) (to Kinetic Properties and Metabolic Contributions of Yeast Mitochondrial and Cytosolic NADP+-specific Isocitrate Dehydrogenases). The reductive carboxylation reaction contained 50 mM potassium phosphate buffer pH 6.5, 0.5 mM NADPH (481973, Merck), 5 mM MgCl2, 40 mM NaHCO3. Reaction was started with an addition of 25 µl of 11 mM α-ketoglutarate (75890, Merck), which gave 1 mM final concentration.

Phosphoenolpyruvate carboxykinase (Pck1, EC 4.1.1.49) activity was measured according to Roja *et. al.* [62]. The assay mixture contained 100 mM HEPES buffer pH 7.5, 0.4 mM NADH (N8129, Sigma Aldrich), 1 mM GTP (G8877, Merck), 1 mM ADP (A2754, Sigma-Aldrich), 4 mM MgCl2, 0.2 mM MnCl2, 0.5 U pyruvate kinase (10128155001, Roche), 0.5 U lactic dehydrogenase (10127876001, Roche) and cell free extract. Reaction was started with an addition of 25 µl of 4.4 mM oxaloacetic acid (OAA, O4126, Merck), to a final concentration of 0.4 mM.

Malate dehydrogenase (Mdh1, Mdh2, Mdh3, EC 1.1.1.37) activity was measured according to Lee et al. 2009 [63]. The assay mixture contained 100 mM potassium phosphate buffer pH 7.4, 3.75 mM NADH (N8129, Sigma-Aldrich) and cell free extract. Reaction was started with an addition of 25 µl of 66 mM oxaloacetic acid (OAA, O4126, Merc), to a final concentration of 6 mM.

NADP+-dependent malic enzyme (Mae1, EC 1.1.1.38) activity was measured according to Boles and co-authors [64]. The assay mixture contained 100 mM Tris-HCl pH 7.5, 10 mM MgCl2, 0.4 mM NADP+ (N5755, Sigma-Aldrich) and cell free extract. Reaction was started with an addition of 25 µl of 110 mM L-malate (M1000, Merc), to a final concentration of 10 mM.

All assays were performed for at least three independent biological replicates. Each biological sample was measured twice in four dilutions. The presented results are mean values with standard deviations obtained for technical and biological replicates. Statistical significance was calculated according to Student's t-test.

5.5. Acetyl-CoA, NAD+ and NADH measurement

To determine acetyl-CoA level, yeast cell extracts were prepared according to Liu, Zhang and Jiang [65]. The amount of acetyl-CoA was determined using the MAK039-1KT fluorometric kit (Sigma-Aldrich), according to the manufacturer's instructions. Acetyl-CoA concentration expressed in ng was calculated from standard curve and standardized to cells dry weight expressed in g. NAD+ and NADH levels were measured according to NAD/NADH Assay Kit II (colorimetric, ab221821, Abcam) as stated in manufacturer's protocol. NAD+ and NADH concentrations expressed in µM was calculated from standard curve and standardized to total proteins concentration expressed in mg. The assays were performed for at least three independent biological replicates.

5.6. Lipid extraction and staining

The extraction and staining of total cellular lipids was done as described by [66,67]. Briefly, 50 ml of yeast cells grown to OD600 ≈ 1.0 either in YPD or YPGly at 30°C or 37°C were harvested by centrifugation, lyophilized and weighted to determine dry cell weight. The lipids were extracted from the lyophilized biomass with chloroform:methanol mixture (2:1, v/v) with Mini-Beadbeater 24 (Biospec products) using 200 µl of glass beads (425– 600 µm; Sigma Aldrich) in 8 bursts of 10 s each with break between the cycles for 1 min incubation on ice. Lipids were recovered by evaporation of the bottom layer solvent and the pellet was weighted. The obtained result is percentage of lipids content in cell dry weight.

Supplementary Materials: The following supporting information can be downloaded at the website of this paper posted on Preprints.org.

Author Contributions: Conceptualization, M.A.; methodology, M.A., R.Sz, C.L.; software, C.L., A.K..; formal analysis, M.A.,C.L, R.Sz, E.F., AK; investigation, M.A., C.L.; resources, M.A., C.L.; data curation, C.L.; writing—

original draft preparation, M.A.; writing—review and editing, M.A., C.L., R.Sz.; visualization, M.A, R.Sz., C.L.; supervision, M.A., C.L; project administration, M.A.; funding acquisition, M.A., R.Sz. All authors have read and agreed to the published version of the manuscript. Authorship must be limited to those who have contributed substantially to the work reported.

Funding: This research was funded by National Science Centre, Poland grant no. 2012/05/E/NZ2/00583 to M.A., EMBO Short-Term Fellowship no. 6069 to R.Sz and by funding from Faculty of Chemistry, Warsaw University of Technology, Poland Nchem2 no.504/04632/1020/43.120012 to R.Sz. and Nchem2 no. 504/04632/1020/43.120010 supporting M.A.

Institutional Review Board Statement: Not applicable.

Informed Consent Statement: Not applicable.

Data Availability Statement: The data presented in this study are available on request from the corresponding author.

Conflicts of Interest: The authors declare no conflict of interest.

References

1. Shen, K.; Pender, C.L.; Bar-Ziv, R.; Zhang, H.; Wickham, K.; Willey, E.; Durieux, J.; Ahmad, Q.; Dillin, A. Mitochondria as Cellular and Organismal Signaling Hubs. *Annu Rev Cell Dev Biol* **2022**, *38*, 179–218, doi:10.1146/annurev-cellbio-120420-015303.
2. Willis, I.M.; Moir, R.D.; Hernandez, N. Metabolic Programming a Lean Phenotype by Deregulation of RNA Polymerase III. *PNAS* **2018**, *115*, 12182–12187, doi:10.1073/pnas.1815590115.
3. Percudani, R.; Pavesi, A.; Ottonello, S. Transfer RNA Gene Redundancy and Translational Selection in Saccharomyces Cerevisiae. *J Mol Biol* **1997**, *268*, 322–330, doi:10.1006/jmbi.1997.0942.
4. Dieci, G.; Fiorino, G.; Castelnuovo, M.; Teichmann, M.; Pagano, A. The Expanding RNA Polymerase III Transcriptome. *Trends in Genetics* **2007**, *23*, 614–622, doi:10.1016/j.tig.2007.09.001.
5. Pluta, K.; Lefebvre, O.; Martin, N.C.; Smagowicz, W.J.; Stanford, D.R.; Ellis, S.R.; Hopper, A.K.; Sentenac, A.; Boguta, M. Maf1p, a Negative Effector of RNA Polymerase III in Saccharomyces Cerevisiae. *Mol Cell Biol* **2001**, *21*, 5031–5040, doi:10.1128/MCB.21.15.5031-5040.2001.
6. Upadhya, R.; Lee, J.; Willis, I.M. Maf1 Is an Essential Mediator of Diverse Signals That Repress RNA Polymerase III Transcription. *Molecular Cell* **2002**, *10*, 1489–1494, doi:10.1016/S1097-2765(02)00787-6.
7. Roberts, D.N.; Wilson, B.; Huff, J.T.; Stewart, A.J.; Cairns, B.R. Dephosphorylation and Genome-Wide Association of Maf1 with Pol III-Transcribed Genes during Repression. *Mol. Cell* **2006**, *22*, 633–644, doi:10.1016/j.molcel.2006.04.009.
8. Vannini, A.; Ringel, R.; Kusser, A.G.; Berninghausen, O.; Kassavetis, G.A.; Cramer, P. Molecular Basis of RNA Polymerase III Transcription Repression by Maf1. *Cell* **2010**, *143*, 59–70, doi:10.1016/j.cell.2010.09.002.
9. Wei, Y.; Tsang, C.K.; Zheng, X.F.S. Mechanisms of Regulation of RNA Polymerase III-Dependent Transcription by TORC1. *EMBO J.* **2009**, *28*, 2220–2230, doi:10.1038/emboj.2009.179.
10. Graczyk, D.; Debski, J.; Muszyńska, G.; Bretner, M.; Lefebvre, O.; Boguta, M. Casein Kinase II-Mediated Phosphorylation of General Repressor Maf1 Triggers RNA Polymerase III Activation. *Proc. Natl. Acad. Sci. U.S.A.* **2011**, *108*, 4926–4931, doi:10.1073/pnas.1010010108.
11. Cai, Y.; Wei, Y.-H. Distinct Regulation of Maf1 for Lifespan Extension by Protein Kinase A and Sch9. *Aging (Albany NY)* **2015**, *7*, 133–143, doi:10.18632/aging.100727.
12. Adamczyk, M.; Szatkowska, R. Low RNA Polymerase III Activity Results in up Regulation of HXT2 Glucose Transporter Independently of Glucose Signaling and despite Changing Environment. *PLoS One* **2017**, *12*, e0185516, doi:10.1371/journal.pone.0185516.
13. Szatkowska, R.; Garcia-Albornoz, M.; Roszkowska, K.; Holman, S.W.; Furmanek, E.; Hubbard, S.J.; Beynon, R.J.; Adamczyk, M. Glycolytic Flux in Saccharomyces Cerevisiae Is Dependent on RNA Polymerase III and Its Negative Regulator Maf1. *Biochem. J.* **2019**, *476*, 1053–1082, doi:10.1042/BCJ20180701.
14. Boguta, M.; Czerska, K.; Zoładek, T. Mutation in a New Gene MAF1 Affects TRNA Suppressor Efficiency in Saccharomyces Cerevisiae. *Gene* **1997**, *185*, 291–296.
15. Willis, I.M. Maf1 Phenotypes and Cell Physiology. *Biochim Biophys Acta Gene Regul Mech* **2018**, *1861*, 330–337, doi:10.1016/j.bbagrm.2017.11.009.

16. Morawiec, E.; Wichtowska, D.; Graczyk, D.; Conesa, C.; Lefebvre, O.; Boguta, M. Maf1, Repressor of TRNA Transcription, Is Involved in the Control of Gluconeogenetic Genes in Saccharomyces Cerevisiae. *Gene* **2013**, *526*, 16–22, doi:10.1016/j.gene.2013.04.055.
17. Cieśla, M.; Towpik, J.; Graczyk, D.; Oficjalska-Pham, D.; Harismendy, O.; Suleau, A.; Balicki, K.; Conesa, C.; Lefebvre, O.; Boguta, M. Maf1 Is Involved in Coupling Carbon Metabolism to RNA Polymerase III Transcription. *Mol Cell Biol* **2007**, *27*, 7693–7702, doi:10.1128/MCB.01051-07.
18. Przybyla-Zawislak, B.; Gadde, D.M.; Ducharme, K.; McCammon, M.T. Genetic and Biochemical Interactions Involving Tricarboxylic Acid Cycle (TCA) Function Using a Collection of Mutants Defective in All TCA Cycle Genes. *Genetics* **1999**, *152*, 153–166.
19. Martínez-Reyes, I.; Chandel, N.S. Mitochondrial TCA Cycle Metabolites Control Physiology and Disease. *Nat Commun* **2020**, *11*, 102, doi:10.1038/s41467-019-13668-3.
20. Yang, C.; Ko, B.; Hensley, C.T.; Jiang, L.; Wasti, A.T.; Kim, J.; Sudderth, J.; Calvaruso, M.A.; Lumata, L.; Mitsche, M.; et al. Glutamine Oxidation Maintains the TCA Cycle and Cell Survival during Impaired Mitochondrial Pyruvate Transport. *Mol Cell* **2014**, *56*, 414–424, doi:10.1016/j.molcel.2014.09.025.
21. Vemuri, G.N.; Eiteman, M.A.; McEwen, J.E.; Olsson, L.; Nielsen, J. Increasing NADH Oxidation Reduces Overflow Metabolism in Saccharomyces Cerevisiae. *Proc Natl Acad Sci U S A* **2007**, *104*, 2402–2407, doi:10.1073/pnas.0607469104.
22. Gaude, E.; Schmidt, C.; Gammage, P.A.; Dugourd, A.; Blacker, T.; Chew, S.P.; Saez-Rodriguez, J.; O'Neill, J.S.; Szabadkai, G.; Minczuk, M.; et al. NADH Shuttling Couples Cytosolic Reductive Carboxylation of Glutamine with Glycolysis in Cells with Mitochondrial Dysfunction. *Mol Cell* **2018**, *69*, 581-593.e7, doi:10.1016/j.molcel.2018.01.034.
23. Schwartz, J.P.; Passonneau, J.V.; Johnson, G.S.; Pastan, I. The Effect of Growth Conditions on NAD+ and NADH Concentrations and the NAD+:NADH Ratio in Normal and Transformed Fibroblasts. *J Biol Chem* **1974**, *249*, 4138–4143.
24. Galdieri, L.; Zhang, T.; Rogerson, D.; Lleshi, R.; Vancura, A. Protein Acetylation and Acetyl Coenzyme a Metabolism in Budding Yeast. *Eukaryot Cell* **2014**, *13*, 1472–1483, doi:10.1128/EC.00189-14.
25. Kuang, Z.; Pinglay, S.; Ji, H.; Boeke, J.D. Msn2/4 Regulate Expression of Glycolytic Enzymes and Control Transition from Quiescence to Growth. *Elife* **2017**, *6*, doi:10.7554/eLife.29938.
26. Khanna, A.; Johnson, D.L.; Curran, S.P. Physiological Roles for Mafr-1 in Reproduction and Lipid Homeostasis. *Cell Rep* **2014**, *9*, 2180–2191, doi:10.1016/j.celrep.2014.11.035.
27. Mierzejewska, J.; Chreptowicz, K. Lack of Maf1 Enhances Pyruvate Kinase Activity and Fermentative Metabolism While Influencing Lipid Homeostasis in Saccharomyces Cerevisiae. *FEBS Lett* **2016**, *590*, 93–100, doi:10.1002/1873-3468.12033.
28. Hammerquist, A.M.; Escorcia, W.; Curran, S.P. Maf1 Regulates Intracellular Lipid Homeostasis in Response to DNA Damage Response Activation. *Mol Biol Cell* **2021**, *32*, 1086–1093, doi:10.1091/mbc.E20-06-0378.
29. Amorim, J.A.; Coppotelli, G.; Rolo, A.P.; Palmeira, C.M.; Ross, J.M.; Sinclair, D.A. Mitochondrial and Metabolic Dysfunction in Ageing and Age-Related Diseases. *Nat Rev Endocrinol* **2022**, *18*, 243–258, doi:10.1038/s41574-021-00626-7.
30. Camarasa, C.; Grivet, J.-P.; Dequin, S. Investigation by 13C-NMR and Tricarboxylic Acid (TCA) Deletion Mutant Analysis of Pathways for Succinate Formation in Saccharomyces Cerevisiae during Anaerobic Fermentation. *Microbiology (Reading)* **2003**, *149*, 2669–2678, doi:10.1099/mic.0.26007-0.
31. *Molecular Mechanisms in Yeast Carbon Metabolism*; Piskur, J., Compagno, C., Eds.; Springer-Verlag: Berlin Heidelberg, 2014; ISBN 978-3-642-55012-6.
32. DeRisi, J.L.; Iyer, V.R.; Brown, P.O. Exploring the Metabolic and Genetic Control of Gene Expression on a Genomic Scale. *Science* **1997**, *278*, 680–686, doi:10.1126/science.278.5338.680.
33. Blank, L.M.; Sauer, U. TCA Cycle Activity in Saccharomyces Cerevisiae Is a Function of the Environmentally Determined Specific Growth and Glucose Uptake Rates. *Microbiology (Reading)* **2004**, *150*, 1085–1093, doi:10.1099/mic.0.26845-0.
34. Lateef, O.M.; Akintubosun, M.O.; Olaoba, O.T.; Samson, S.O.; Adamczyk, M. Making Sense of "Nonsense" and More: Challenges and Opportunities in the Genetic Code Expansion, in the World of TRNA Modifications. *Int J Mol Sci* **2022**, *23*, 938, doi:10.3390/ijms23020938.
35. Pietrocola, F.; Galluzzi, L.; Bravo-San Pedro, J.M.; Madeo, F.; Kroemer, G. Acetyl Coenzyme A: A Central Metabolite and Second Messenger. *Cell Metab* **2015**, *21*, 805–821, doi:10.1016/j.cmet.2015.05.014.

36. Palian, B.M.; Rohira, A.D.; Johnson, S.A.S.; He, L.; Zheng, N.; Dubeau, L.; Stiles, B.L.; Johnson, D.L. Maf1 Is a Novel Target of PTEN and PI3K Signaling That Negatively Regulates Oncogenesis and Lipid Metabolism. *PLOS Genetics* **2014**, *10*, e1004789, doi:10.1371/journal.pgen.1004789.
37. Wise, D.R.; Thompson, C.B. Glutamine Addiction: A New Therapeutic Target in Cancer. *Trends Biochem Sci* **2010**, *35*, 427–433, doi:10.1016/j.tibs.2010.05.003.
38. DeBerardinis, R.J.; Lum, J.J.; Hatzivassiliou, G.; Thompson, C.B. The Biology of Cancer: Metabolic Reprogramming Fuels Cell Growth and Proliferation. *Cell Metab* **2008**, *7*, 11–20, doi:10.1016/j.cmet.2007.10.002.
39. Metallo, C.M.; Gameiro, P.A.; Bell, E.L.; Mattaini, K.R.; Yang, J.; Hiller, K.; Jewell, C.M.; Johnson, Z.R.; Irvine, D.J.; Guarente, L.; et al. Reductive Glutamine Metabolism by IDH1 Mediates Lipogenesis under Hypoxia. *Nature* **2011**, *481*, 380–384, doi:10.1038/nature10602.
40. Yoo, H.; Antoniewicz, M.R.; Stephanopoulos, G.; Kelleher, J.K. Quantifying Reductive Carboxylation Flux of Glutamine to Lipid in a Brown Adipocyte Cell Line. *J Biol Chem* **2008**, *283*, 20621–20627, doi:10.1074/jbc.M706494200.
41. Katz, A.; Elgamal, S.; Rajkovic, A.; Ibba, M. Non-Canonical Roles of TRNAs and TRNA Mimics in Bacterial Cell Biology. *Mol Microbiol* **2016**, *101*, 545–558, doi:10.1111/mmi.13419.
42. Michanek, A.; Kristen, N.; Höök, F.; Nylander, T.; Sparr, E. RNA and DNA Interactions with Zwitterionic and Charged Lipid Membranes - a DSC and QCM-D Study. *Biochim Biophys Acta* **2010**, *1798*, 829–838, doi:10.1016/j.bbamem.2009.12.009.
43. Czerniak, T.; Saenz, J.P. Lipid Membranes Modulate the Activity of RNA through Sequence-Dependent Interactions. *Proc Natl Acad Sci U S A* **2022**, *119*, e2119235119, doi:10.1073/pnas.2119235119.
44. Gombert, A.K.; Moreira dos Santos, M.; Christensen, B.; Nielsen, J. Network Identification and Flux Quantification in the Central Metabolism of Saccharomyces Cerevisiae under Different Conditions of Glucose Repression. *J Bacteriol* **2001**, *183*, 1441–1451, doi:10.1128/JB.183.4.1441-1451.2001.
45. Fernandez-de-Cossio-Diaz, J.; Vazquez, A. Limits of Aerobic Metabolism in Cancer Cells. *Sci Rep* **2017**, *7*, 13488, doi:10.1038/s41598-017-14071-y.
46. Al-Dwairi, A.; Pabona, J.M.P.; Simmen, R.C.M.; Simmen, F.A. Cytosolic Malic Enzyme 1 (ME1) Mediates High Fat Diet-Induced Adiposity, Endocrine Profile, and Gastrointestinal Tract Proliferation-Associated Biomarkers in Male Mice. *PLoS One* **2012**, *7*, e46716, doi:10.1371/journal.pone.0046716.
47. Simmen, F.A.; Alhallak, I.; Simmen, R.C.M. Malic Enzyme 1 (ME1) in the Biology of Cancer: It Is Not Just Intermediary Metabolism. *J Mol Endocrinol* **2020**, *65*, R77–R90, doi:10.1530/JME-20-0176.
48. Fan, J.; Ye, J.; Kamphorst, J.J.; Shlomi, T.; Thompson, C.B.; Rabinowitz, J.D. Quantitative Flux Analysis Reveals Folate-Dependent NADPH Production. *Nature* **2014**, *510*, 298–302, doi:10.1038/nature13236.
49. Nakashima, C.; Kirita, T.; Yamamoto, K.; Mori, S.; Luo, Y.; Sasaki, T.; Fujii, K.; Ohmori, H.; Kawahara, I.; Mori, T.; et al. Malic Enzyme 1 Is Associated with Tumor Budding in Oral Squamous Cell Carcinomas. *Int J Mol Sci* **2020**, *21*, 7149, doi:10.3390/ijms21197149.
50. Easlon, E.; Tsang, F.; Skinner, C.; Wang, C.; Lin, S.-J. The Malate-Aspartate NADH Shuttle Components Are Novel Metabolic Longevity Regulators Required for Calorie Restriction-Mediated Life Span Extension in Yeast. *Genes Dev* **2008**, *22*, 931–944, doi:10.1101/gad.1648308.
51. Heyland, J.; Fu, J.; Blank, L.M. Correlation between TCA Cycle Flux and Glucose Uptake Rate during Respiro-Fermentative Growth of Saccharomyces Cerevisiae. *Microbiology (Reading)* **2009**, *155*, 3827–3837, doi:10.1099/mic.0.030213-0.
52. Blank, L.M.; Kuepfer, L.; Sauer, U. Large-Scale 13C-Flux Analysis Reveals Mechanistic Principles of Metabolic Network Robustness to Null Mutations in Yeast. *Genome Biol* **2005**, *6*, R49, doi:10.1186/gb-2005-6-6-r49.
53. Orekhov, V.Y.; Jaravine, V.A. Analysis of Non-Uniformly Sampled Spectra with Multi-Dimensional Decomposition. *Prog Nucl Magn Reson Spectrosc* **2011**, *59*, 271–292, doi:10.1016/j.pnmrs.2011.02.002.
54. Kazimierczuk, K.; Orekhov, V.Y. Accelerated NMR Spectroscopy by Using Compressed Sensing. *Angew Chem Int Ed Engl* **2011**, *50*, 5556–5559, doi:10.1002/anie.201100370.
55. Delaglio, F.; Grzesiek, S.; Vuister, G.W.; Zhu, G.; Pfeifer, J.; Bax, A. NMRPipe: A Multidimensional Spectral Processing System Based on UNIX Pipes. *J Biomol NMR* **1995**, *6*, 277–293, doi:10.1007/BF00197809.
56. Ludwig, C.; Günther, U.L. MetaboLab--Advanced NMR Data Processing and Analysis for Metabolomics. *BMC Bioinformatics* **2011**, *12*, 366, doi:10.1186/1471-2105-12-366.

57. Chong, M.; Jayaraman, A.; Marin, S.; Selivanov, V.; de Atauri Carulla, P.R.; Tennant, D.A.; Cascante, M.; Günther, U.L.; Ludwig, C. Combined Analysis of NMR and MS Spectra (CANMS). *Angewandte Chemie International Edition* **2017**, *56*, 4140–4144, doi:https://doi.org/10.1002/anie.201611634.
58. Heavner, B.D.; Price, N.D. Comparative Analysis of Yeast Metabolic Network Models Highlights Progress, Opportunities for Metabolic Reconstruction. *PLoS Comput Biol* **2015**, *11*, e1004530, doi:10.1371/journal.pcbi.1004530.
59. Adamczyk, M.; van Eunen, K.; Bakker, B.M.; Westerhoff, H.V. Enzyme Kinetics for Systems Biology. *Methods in Enzymology* **2011**, *500*, 233–257, doi:10.1016/B978-0-12-385118-5.00013-X.
60. Lin, A.-P.; Demeler, B.; Minard, K.I.; Anderson, S.L.; Schirf, V.; Galaleldeen, A.; McAlister-Henn, L. Construction and Analyses of Tetrameric Forms of Yeast NAD+-Specific Isocitrate Dehydrogenase. *Biochemistry* **2011**, *50*, 230–239, doi:10.1021/bi101401h.
61. Contreras-Shannon, V.; Lin, A.-P.; McCammon, M.T.; McAlister-Henn, L. Kinetic Properties and Metabolic Contributions of Yeast Mitochondrial and Cytosolic NADP+-Specific Isocitrate Dehydrogenases. *J Biol Chem* **2005**, *280*, 4469–4475, doi:10.1074/jbc.M410140200.
62. Rojas, B.E.; Hartman, M.D.; Figueroa, C.M.; Leaden, L.; Podestá, F.E.; Iglesias, A.A. Biochemical Characterization of Phosphoenolpyruvate Carboxykinases from Arabidopsis Thaliana. *Biochem J* **2019**, *476*, 2939–2952, doi:10.1042/BCJ20190523.
63. Lee, S.M.; Kim, J.H.; Cho, E.J.; Youn, H.D. A Nucleocytoplasmic Malate Dehydrogenase Regulates P53 Transcriptional Activity in Response to Metabolic Stress. *Cell Death Differ* **2009**, *16*, 738–748, doi:10.1038/cdd.2009.5.
64. Boles, E.; de Jong-Gubbels, P.; Pronk, J.T. Identification and Characterization of MAE1, the Saccharomyces Cerevisiae Structural Gene Encoding Mitochondrial Malic Enzyme. *J Bacteriol* **1998**, *180*, 2875–2882, doi:10.1128/JB.180.11.2875-2882.1998.
65. Liu, W.; Zhang, B.; Jiang, R. Improving Acetyl-CoA Biosynthesis in Saccharomyces Cerevisiae via the Overexpression of Pantothenate Kinase and PDH Bypass. *Biotechnol Biofuels* **2017**, *10*, 41, doi:10.1186/s13068-017-0726-z.
66. Wolinski, H.; Kohlwein, S.D. Microscopic Analysis of Lipid Droplet Metabolism and Dynamics in Yeast. *Methods Mol Biol* **2008**, *457*, 151–163, doi:10.1007/978-1-59745-261-8_11.
67. Bligh, E.G.; Dyer, W.J. A Rapid Method of Total Lipid Extraction and Purification. *Can J Biochem Physiol* **1959**, *37*, 911–917, doi:10.1139/o59-099.